






Prohibitin 1 regulates mtDNA release and downstream inflammatory responses

Hao Liu^{1,2,3,†} , Hualin Fan^{2,4,†}, Pengcheng He^{5,6,7,8,†}, Haixia Zhuang⁹, Xiao Liu², Meiting Chen¹⁰, Wenwei Zhong² , Yi Zhang^{2,11} , Cien Zhen^{2,4}, Yanling Li¹⁰ , Huilin Jiang¹⁰, Tian Meng², Yiming Xu^{1,2,3}, Guojun Zhao¹ & Du Feng^{1,2,3,*} 

Abstract

Exposure of mitochondrial DNA (mtDNA) to the cytosol activates innate immune responses. But the mechanisms by which mtDNA crosses the inner mitochondrial membrane are unknown. Here, we found that the inner mitochondrial membrane protein prohibitin 1 (PHB1) plays a critical role in mtDNA release by regulating permeability across the mitochondrial inner membrane. Loss of PHB1 results in alterations in mitochondrial integrity and function. PHB1-deficient macrophages, serum from myeloid-specific PHB1 KO (Phb1MyeKO) mice, and peripheral blood mononuclear cells from neonatal sepsis patients show increased interleukin-1 β (IL-1 β) levels. PHB1 KO mice are also intolerant of lipopolysaccharide shock. Phb1-depleted macrophages show increased cytoplasmic release of mtDNA and inflammatory responses. This process is suppressed by cyclosporine A and VBIT-4, which inhibit the mitochondrial permeability transition pore (mPTP) and VDAC oligomerization. Inflammatory stresses downregulate PHB1 expression levels in macrophages. Under normal physiological conditions, the inner mitochondrial membrane proteins, AFG3L2 and SPG7, are tethered to PHB1 to inhibit mPTP opening. Downregulation of PHB1 results in enhanced interaction between AFG3L2 and SPG7, mPTP opening, mtDNA release, and downstream inflammatory responses.

Keywords AFG3L2; MIMP; mtDNA; PHB; SPG7

Subject Categories Immunology; Organelles

DOI 10.15252/embj.2022111173 | Received 15 March 2022 | Revised 11

September 2022 | Accepted 14 September 2022 | Published online 17 October 2022

The EMBO Journal (2022) 41: e111173

Introduction

The mitochondrion plays an important role in immunity, and it harbors contents serving as effective agonists of inflammation, the most notable of which is mtDNA (West & Shadel, 2017). Previous studies have reported that the release of mtDNA into the cytoplasm triggers innate immunity and inflammation (Kim *et al*, 2019; Wang *et al*, 2021). In response to cytosolic exposure of mtDNA, two major DNA-sensing signaling pathways will be activated: one is the cyclic GMP-AMP synthase-Stimulator of interferon genes protein (cGAS-STING) pathway, and the other is the inflammasome pathway (Kim *et al*, 2019; Wang *et al*, 2021). In the cGAS-STING pathway, double-stranded DNA exposed to the cytosol will bind to cGAS, which in turn activates STING and subsequently causes phosphorylation of TANK-binding kinase 1 (TBK1) and IFN regulatory factor 3 (IRF3), resulting in the induction of type I interferon (Wu *et al*, 2013). In the inflammasome pathway, several pattern recognition receptors, such as NOD, LRR, and Pyrin domain-containing protein 3 (NLRP3) and absent in melanoma 2 (AIM2), oligomerize and bind to the adaptor molecule ASC and the effector molecule pro-caspase-1 under the stimulation of pathogen-associated molecular patterns (PAMPs) or damage-associated molecular pattern (DAMPs) (Schroder & Tschopp, 2010). Consequently, pro-caspase-1 is cleaved to the mature form of caspase-1, which then cleaves pro-interleukin-1 β (IL-1 β) and Gasdermin D to promote the pro-inflammatory process and pyroptosis (Swanson *et al*, 2019). The activation of inflammasomes is associated with several diseases, including sepsis, atherosclerosis, diabetes, and neurodegeneration (Swanson *et al*, 2019). Although it is widely known that mtDNA release is required for inflammatory responses (Shimada *et al*, 2012), the exact

1 Qingyuan People's Hospital, The Sixth Affiliated Hospital of Guangzhou Medical University, Qingyuan, China

2 Guangzhou Municipal and Guangdong Provincial Key Laboratory of Protein Modification and Degradation, School of Basic Medical Sciences, Affiliated Cancer Hospital and Institute of Guangzhou Medical University, Guangzhou Medical University, Guangzhou, China

3 State Key Laboratory of Respiratory Disease, Guangzhou Medical University, Guangzhou, China

4 Department of Cardiology, School of Medicine, South China University of Technology, Guangzhou, China

5 Department of Cardiology, Guangdong Cardiovascular Institute, Guangdong Provincial People's Hospital, Guangdong Academy of Medical Sciences, Guangzhou, China

6 Guangdong Provincial Key Laboratory of Coronary Heart Disease Prevention, Guangdong Provincial People's Hospital, Guangdong Academy of Medical Sciences, Guangzhou, China

7 Guangdong Provincial People's Hospital, Guangdong Academy of Medical Sciences, School of Medicine, South China University of Technology, Guangzhou, China

8 Department of Cardiology, Heyuan People's Hospital, Heyuan, China

9 Department of Anesthesiology, Second Clinical College of Guangzhou Medical University, Guangzhou, China

10 Emergency Department, The Second Affiliated Hospital of Guangzhou Medical University, Guangzhou, China

11 GMU-GIBH Joint School of Life Sciences, Guangzhou Medical University, Guangzhou, China

*Corresponding author. Tel: +86 020 37105192; E-mail: fenglab@gzhmu.edu.cn

†These authors contributed equally to this work

mechanism of how mtDNA is released from mitochondria into the cytoplasm remains enigmatic.

Perturbations in mitochondrial outer and inner membrane permeability (MOMP and MIMP) are the main causes of mtDNA release (Riley & Tait, 2020). Cumulative evidence has revealed that mtDNA effluxes through the outer mitochondrial membrane via mechanisms involving voltage-dependent anion channel (VDAC) oligomers and BCL2 antagonist/killer and BCL2 associated X, apoptosis regulator (BAK/BAX) macropores (McArthur et al, 2018; Kim et al, 2019). Upon MOMP transition, short mtDNA fragments are released into the cytosol through VDAC oligomers in cells lacking mitochondrial endonuclease G (Kim et al, 2019). During cellular apoptosis, mtDNA is released into the cytosol through BAK/BAX macropores (McArthur et al, 2018; Riley et al, 2018). Unfortunately, the clear mechanism of MIMP releasing mtDNA remains to be elucidated. On the inner mitochondrial membrane, several proteins contribute to the formation and opening of mPTP (Izzo et al, 2016), which participates in mtDNA release that triggers the inflammatory response (Yu et al, 2020; Wang et al, 2021). However, the specific proteins that regulate the opening of mPTP for mtDNA release remain unclear.

Several proteins localized in the mitochondrial inner membrane were reported to be components of mPTP and regulate MIMP, including adenine nucleotide translocase (ANT) (Woodfield et al, 1998), the F1Fo ATP synthase (Bonora et al, 2013; Giorgio et al, 2013), and spastic paraplegia 7 protein (SPG7) (Shanmughapriya et al, 2015). These factors are thought to be required for the opening of mPTP to mediate ion transport between the cytosol and the mitochondrial matrix (Bonora et al, 2021). However, it remains unclear how these factors are coordinated to regulate MIMP and to promote mtDNA release through the inner mitochondrial membrane.

Prohibitin (PHB) 1 is localized to the inner mitochondrial membrane and interacts with PHB2. Approximately 12 to 16 heterodimers form a ring-shaped complex that maintains mitochondrial structure and function (Artal-Sanz & Tavernarakis, 2009). Kasashima et al (2008) reported that loss of PHB1 impaired the organization of mitochondrial nucleoids (mtDNA/protein complexes) and reduced the level of the core nucleoid component, mitochondrial transcription factor A (TFAM). These disorders in mitochondrial nucleoids result in a decrease in the copy number of mtDNA (Kasashima et al, 2008). Furthermore, He et al (2012) isolated mitochondrial nucleoids and found PHB1 in the nucleoid fraction. Thus, PHB1 was proposed to be a possible component of mitochondrial nucleoids. In addition, PHB1 deficiency has been reported to promote inflammation and increase sensitivity to liver injury (Ko et al, 2010). Mice with intestinal epithelial cell deletion of *Phb1* exhibit spontaneous ileal inflammation (Jackson et al, 2020). However, the mechanistic link between PHB1 perturbation, mtDNA release, and inflammation has not been revealed.

The *m*-AAA protease complex is assembled in a heterohexamer form with AFG3-like protein 2 (AFG3L2) and SPG7 or in a homohexamer form with only AFG3L2 (Levytskyy et al, 2017). Knockdown of SPG7, the potential regulator of mPTP, impairs ion efflux from mitochondria to cytosol (Shanmughapriya et al, 2015). In addition, SPG7 has been demonstrated to interact with cyclophilin D (CYPD), an essential component of mPTP (Crompton et al, 1998; Shanmughapriya et al, 2015). PHB1 may negatively regulate the proteolysis activity of the *m*-AAA protease complex to mediate the

degradation of mitochondrial proteins (Steglich et al, 1999). This raised the question of whether PHB1 promotes mtDNA release by regulating SPG7-CYPD-dependent opening of mPTP. Here, we propose that PHB1 may be a potential factor that localizes in the mitochondrial inner membrane to regulate mtDNA release in response to inflammatory stresses.

Results

Loss of *Phb1* induces inflammation *in vivo* and *in vitro*

Phb1^{-/-} mice were not obtained from heterozygous intercrosses at the expected Mendelian ratio (Appendix Fig S1A). Therefore, we crossed *Phb1*^{F/F} and *LysM-Cre* mice to generate *Phb1*^{F/F}; *LysM-Cre* mice (hereafter called *Phb1*^{MyeKO}) that lack *Phb1* in mature myeloid cells, including macrophages and neutrophils (Appendix Fig S1B). Myeloid cells were extracted from the bone marrow of *Phb1*^{MyeKO} mice and differentiated into bone marrow-derived macrophages (BMDMs). *Phb1* was not expressed in these cells (Appendix Fig S1C and D). Surprisingly, when we performed phenotypic screening on the genetically manipulated mice, we found that the serum level of IL-1β is spontaneously increased in *Phb1*^{MyeKO} mice relative to *Phb1*^{F/F} mice (Fig 1A). After LPS administration, serological IL-1β is increased in both *Phb1*^{F/F} mice and *Phb1*^{MyeKO} mice, and the increase is more pronounced in *Phb1*^{MyeKO} mice (Fig 1A). Accordingly, BMDMs extracted from *Phb1*^{MyeKO} mice have a higher level of cleaved IL-1β relative to BMDMs from *Phb1*^{F/F} mice (Fig 1B). When lipopolysaccharide (LPS)-primed BMDMs are extracted from *Phb1*^{MyeKO} mice and activated by addition of ATP, they secrete more cleaved Caspase-1 and mature IL-1β into the culture medium (Fig 1B and C). Subsequently, we examined the survival rate of mice treated with a high dose of LPS to induce septic shock. We found that the survival rate of *Phb1*^{MyeKO} mice is much lower than *Phb1*^{F/F} mice (Fig 1D).

Sepsis is a clinically common disease typically characterized by a systemic inflammatory response of the human body (Angus & van der Poll, 2013). Guo et al (2020) found that PHB1 mRNA levels in peripheral blood mononuclear cells (PBMCs) were lower in patients with sepsis than in healthy controls. To confirm the connection between PHB1 and this severe inflammatory disease, we extracted PBMCs from infant patients with sepsis and found that the transcription levels of *IL1B* and *IL6* are upregulated in these cells (Fig 1E). The transcription and protein levels of PHB1 are decreased in PBMCs from infant sepsis patients, while the PHB2 levels are relatively stable (Fig 1F).

Based on the observations *in vivo*, we used LPS and ATP stimuli to generate a cellular inflammatory model to further investigate whether PHB1 participates in innate immune responses. Similar to the data collected from PBMCs in infant patients with sepsis, synergistic stimulation of cells from the macrophage cell line J774A.1 with LPS enhances the transcription of *Il1b* and *Il6* (Fig 1G). The mRNA and protein levels of PHB1 but not PHB2 are decreased in the same batch of cell lysate pre-split into two parts (Fig 1G). Consistently, like LPS, exogenous IL-1β also triggers MyD88-signaling to increase transcription of *Il1b* and *Il6*, with a similar effect of LPS on PHB1 mRNA levels in J774A.1 (Fig 1G and H). Of note, the direct stimulation of IL-1β mildly increases the PHB2 mRNA levels

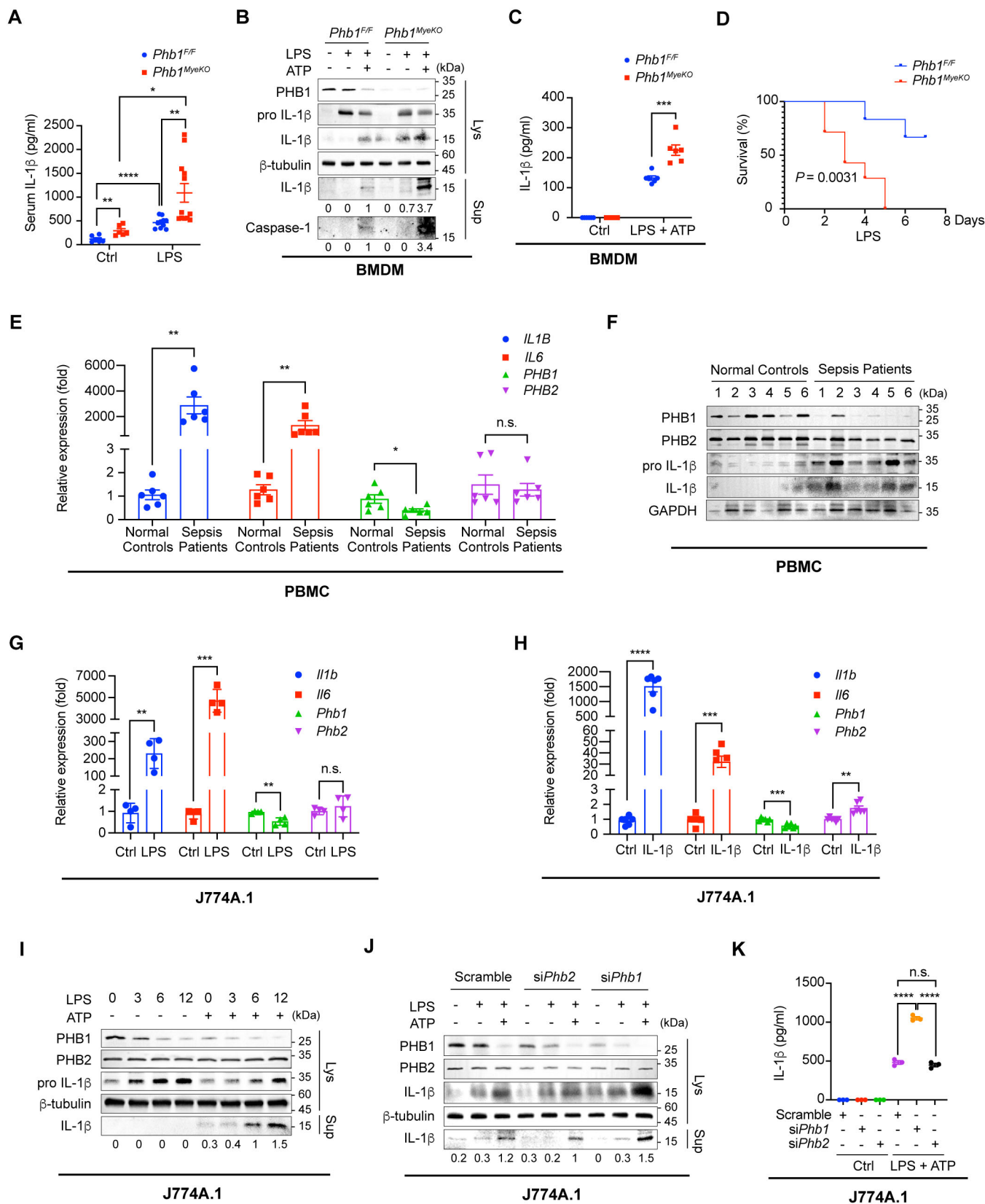


Figure 1.

Figure 1. Loss of *Phb1* induces inflammation *in vivo* and *in vitro*.

- A After being randomized, 8- to 12-week-old and sex-matched *Phb1^{Fl/Fl}* mice and *Phb1^{MyeKO}* mice were administered with PBS or LPS (30 mg/kg) for 12 h via intraperitoneal injection. Serum was collected and ELISA assays were used to detect the level of IL-1 β ($n = 6, 10, 6,$ and 12 mice for each group, respectively). Data presented as mean \pm SEM. * $P < 0.05$, ** $P < 0.01$, **** $P < 0.0001$ (Student's t -test).
- B BMDMs were extracted from *Phb1^{Fl/Fl}* or *Phb1^{MyeKO}* mice and stimulated by 20% culture supernatant of L929 cells for 7 days. Differentiated BMDMs were stimulated with LPS (200 ng/ml) for 6 h and ATP (4 mM) for 45 min, the cells were lysed and the culture medium was collected. Western blotting (WB) assays were used to detect protein levels in whole cell lysates (Lys) and culture medium (Sup).
- C BMDMs were extracted from *Phb1^{Fl/Fl}* or *Phb1^{MyeKO}* mice and stimulated with 20% culture supernatant of L929 cells for 7 days. Differentiated BMDMs were stimulated with LPS (200 ng/ml) for 6 h and ATP (4 mM) for 45 min. ELISA assays were used to detect protein levels in the culture medium. Data of BMDMs from the separate mice ($n = 6$ mice for each group) are presented as mean \pm SEM. *** $P < 0.001$ (Student's t -test).
- D After randomized, 4 weeks old and sex-matched *Phb1^{Fl/Fl}* mice and *Phb1^{MyeKO}* mice were administered with PBS or LPS (300 mg/kg) to induce septic shock via intraperitoneal injection. The life span of *Phb1^{Fl/Fl}* mice ($n = 6$) and *Phb1^{MyeKO}* mice ($n = 7$) was recorded.
- E PBMCs were extracted from normal controls and patients with sepsis. Intracellular mRNA levels were detected by real-time quantitative PCR (RT-qPCR) assays (mean \pm SEM). n.s., no significance, * $P < 0.05$, ** $P < 0.01$ (Student's t -test).
- F PBMCs were extracted from normal controls and infant patients with sepsis. Protein levels in whole cell lysates were detected by WB assays.
- G, H J774A.1 cells were stimulated with LPS (200 ng/ml) for 6 h or recombinant IL-1 β (100 pg/ml) for 24 h. Intracellular mRNA levels were detected by RT-qPCR assays. Data are from four independent experiments for (G) and six independent experiments for (H) (mean \pm SEM). n.s., no significance, ** $P < 0.01$, **** $P < 0.001$, **** $P < 0.0001$ (Student's t -test).
- I After J774A.1 cells were stimulated with LPS (200 ng/ml) for 0, 3, 6, 12 h and ATP (4 mM) for 45 min, the cells were lysed, and the culture medium was collected. Protein levels in whole cell lysates (Lys) and culture medium (Sup) were detected by WB assays.
- J After J774A.1 cells with *Phb1* or *Phb2* knockdown were stimulated with LPS (200 ng/ml) for 6 h and ATP (4 mM) for 45 min, the cells were lysed, and the culture medium was collected. Protein levels in whole cell lysates (Lys) and culture medium (Sup) were detected by WB assays.
- K After J774A.1 cells with *Phb1* or *Phb2* knockdown were stimulated with LPS (200 ng/ml) for 6 h and ATP (4 mM) for 45 min, the culture medium was collected. ELISA assays were used to detect IL-1 β levels in the culture medium. Data are from three independent experiments (mean \pm SEM). n.s., no significance, **** $P < 0.0001$ (Student's t -test).

Source data are available online for this figure.

(Fig 1H). In addition, significantly elevated secretion of IL-1 β into the supernatant is detected after co-stimulation with LPS and ATP (Fig 1I). We found that small interfering RNA (siRNA) knockdown of *Phb1* in LPS + ATP-stimulated J774A.1 macrophages also increases the secretion of IL-1 β into the supernatant, whereas knockdown of *Phb2* does not promote the production of cleaved IL-1 β (Fig 1J and K).

Loss of PHB1 disturbs mitochondrial homeostasis and induces membrane permeability

PHB1 has been reported to maintain multiple mitochondrial functions, including *m*-AAA protease activity (Steglich *et al*, 1999), oxidative phosphorylation (Bourges *et al*, 2004; Jian *et al*, 2017), cristae shape (Kong *et al*, 2014), and the copy number of mitochondrial DNA (Kasashima *et al*, 2008). Consistent with previous studies, we confirmed the major localization of PHB1 to mitochondria in immune and nonimmune cells (Appendix Fig S2A). We generated a HeLa cell line with stable knockdown (KD) of *Phb1*. Single cell-expressing shRNA was selected with GFP⁺, and reduction in PHB1 expression was confirmed by Western blotting (Appendix Fig S2B). In cells with *Phb1* deficiency, we observed the disorders in the mitochondrial network and excessive fragmentation of mitochondria indicated by increased circular- or dot-shaped mitochondrial staining patterns (Fig 2A).

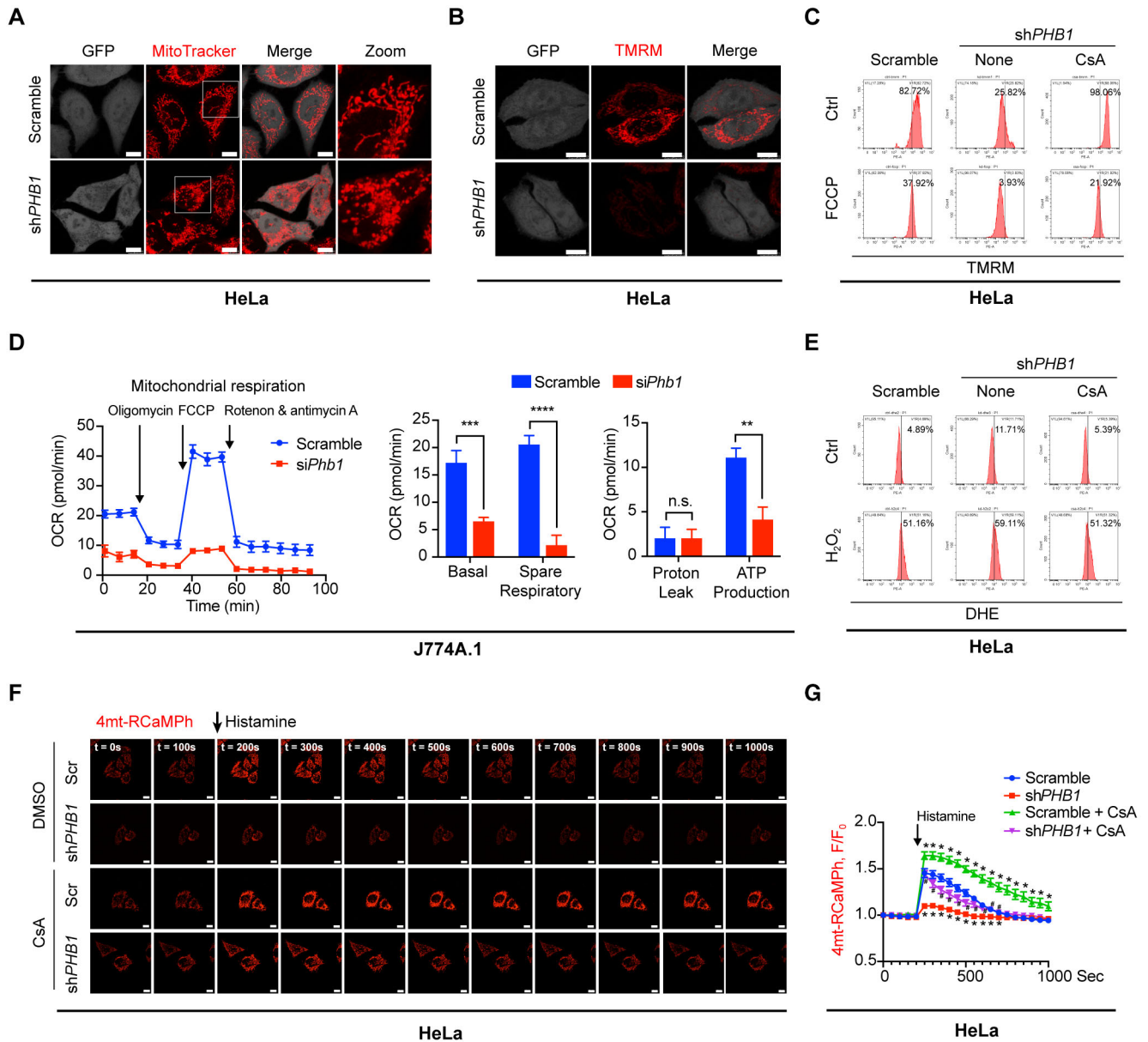
Next, we detected mitochondrial membrane potential ($\Delta\Psi$ m) in the *Phb1* KD HeLa cells with tetramethylrhodamine methyl ester (TMRM), a fluorescent dye that usually accumulates in the mitochondrial matrix of intact mitochondria (Perry *et al*, 2011). We found that $\Delta\Psi$ m is lost upon knockdown of *Phb1* (Fig 2B and C). Given that the opening of mPTP may be attributed to the loss of $\Delta\Psi$ m (Perry *et al*, 2011), we blocked the opening of mPTP by the inhibitor of CYPD, cyclosporin A (CsA). We found that the loss of

$\Delta\Psi$ m caused by *Phb1* deficiency was inhibited by treatment with CsA (Fig 2B and C). As a control, $\Delta\Psi$ m is lost when cells are treated with Carbonyl cyanide 4-(trifluoromethoxy) phenylhydrazone (FCCP), which impairs the mitochondrial electron transport chain (ETC) and proton flux (Fig 2C). This indicates that PHB1 is required for maintenance of $\Delta\Psi$ m, and PHB1 maintains $\Delta\Psi$ m by inhibiting the opening of mPTP and MIMP (Fig 2C).

To investigate whether PHB1 participates in the functions of ETC, we examined mitochondrial respiration. Knockdown of PHB1 decreases the basal oxygen consumption rate, the respiratory capacity, and the ATP production of mitochondria in J774.1 cells (Fig 2D). Additionally, knockdown of *Phb1* increases the production of reactive oxygen species (ROS) under physiological or H₂O₂ stress conditions, while the treatment of CsA restores this excessive production (Fig 2E).

Given that the opening of mPTP impacts mitochondrial Ca²⁺ transient, we further investigated whether PHB1 regulates mitochondrial Ca²⁺ uptake. We examined the mitochondrial Ca²⁺ transient in the *Phb1* KD HeLa cell line stably expressing a Ca²⁺ indicator, 4mt-RCaMP. As described previously (Zhao *et al*, 2019), the fluorescence intensity of 4mt-RCaMP reflects the free Ca²⁺ level in mitochondria. Histamine triggers rapid Ca²⁺ influx from the cytoplasm into mitochondria (Zhao *et al*, 2019). We found that *Phb1* knockdown impairs the uptake of Ca²⁺ in mitochondria, and this impairment is ameliorated by the mPTP inhibitor CsA (Fig 2F and G, Movies EV1–EV4). CsA was not considered that impacts mitochondrial Ca²⁺ uptake (Yun *et al*, 2014), so this amelioration may be attributed to preventing the effects of *Phb1* deficiency on other events and to transiently increasing mitochondrial Ca²⁺ level.

Of note, *Phb1* knockdown does not cause excessive cell death under physiological or oxidative stress conditions compared with the scramble control (Appendix Fig S2C).



PHB1 deficiency promotes mtDNA release via CYPD- and VDAC-associated mPTP opening

Given that the loss of PHB1 promotes the opening of mPTP, we wanted to know whether mtDNA escapes from mitochondria under the same conditions. Using SG-ALK (Han *et al*, 2020) and an anti-DNA antibody (Yu *et al*, 2020) to indicate DNA, we found that knockdown of *Phb1* but not *Phb2* decreases the co-localization between mtDNA and mitochondria in J774.1 cells (Fig 3A and B; Appendix Fig S3A). As described in a previous study (Yu *et al*, 2020), we detected mtDNA levels in the cytosol with qPCR assays and found that PHB1 deficiency enhances the abundance of cytoplasmic mtDNA in J774.1 cells (Fig 3C; Appendix Fig S3B).

To further evaluate mtDNA release upon PHB1 knockout, we extracted the myeloid cells from the bone marrow of *Phb1*^{MyeKO} mice and induced them to differentiate into BMDMs. Consistent with the observations in J774A.1 cells, the co-localization between mtDNA and mitochondria is impaired in BMDMs (Fig 3D and E; Appendix Fig S3C). In addition, PBMCs from *Phb1*^{MyeKO} mice show an increased abundance of cytoplasmic mtDNA (Fig 3F). In nonimmune HeLa cells, *Phb1* knockdown also impairs the co-localization between mtDNA and mitochondria, and enhances the cytoplasmic mtDNA level in nonimmune HeLa cells (Fig 3G and H; Appendix Fig S3D–H). The effects of *Phb1* knockdown are also inhibited by CsA, as evidenced by multiple probes to indicate DNA, including TFAM, SG-ALK, and anti-DNA antibody (Fig 3G and H; Appendix Fig S3D and E).

H₂O₂ is an established activator of mPTP opening. It also induces the oligomerization of VDAC (Keinan *et al*, 2010; Kim *et al*, 2019). When incubated with H₂O₂, HeLa cells showed an increased cytoplasmic mtDNA level (Fig 3I). When the cells are treated with H₂O₂

and CsA, the level of mtDNA within mitochondria is mostly restored (Fig 3I). Accordingly, confocal microscopy shows that the co-localization between mtDNA and mitochondria is reduced in response to H₂O₂, whereas CsA blocked the H₂O₂-induced efflux of mtDNA (Appendix Fig S4A). By monitoring Ca²⁺ levels in the mitochondrial matrix, we confirmed that H₂O₂ stimulation, comparable with *Phb1* silencing, impairs Ca²⁺ transient in mitochondria (Appendix Fig S4B and C).

Importantly, VBIT-4, an inhibitor of the mitochondrial outer membrane protein VDAC, also suppresses the release of mtDNA caused by *Phb1* knockdown both in immune cells and nonimmune cells (Fig 3J and K).

Phb1 deficiency promotes the assembly of inflammasomes

Previous studies reported that the activation of NLRP3-inflammasomes contributes to the progression of sepsis (Jin *et al*, 2017; Ren *et al*, 2021). Thus, we asked whether PHB1 deficiency promotes the activation of NLRP3-inflammasomes in sepsis. In J774A.1 cells, *Phb1* knockdown enhances the interaction between NLRP3 and ASC, two key components required for inflammasome assembly but does not alter the expression of either of them (Fig 3L).

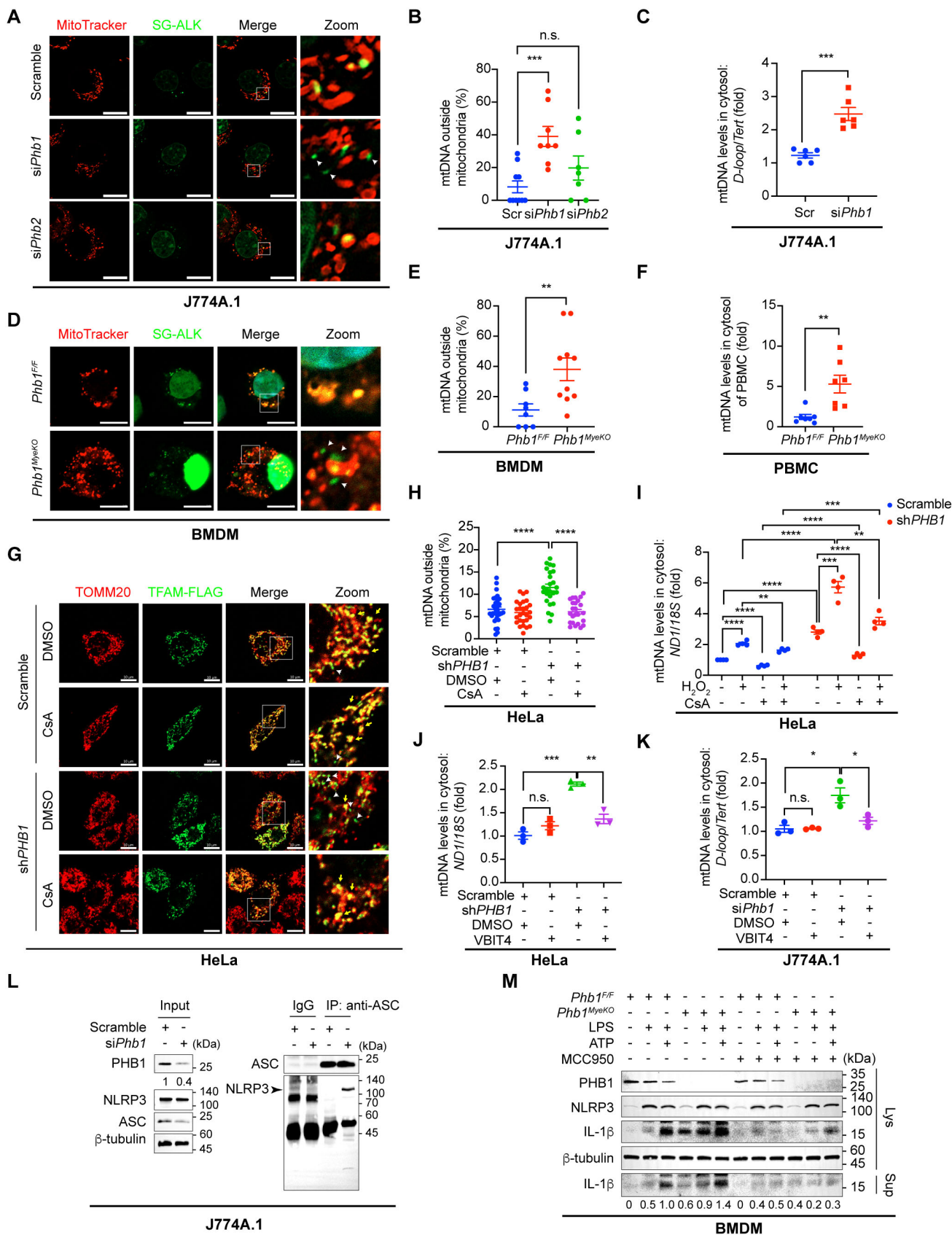
To investigate whether the formation of the NLRP3-inflammasome is the major reason for IL-1 β cleavage promoted by loss of PHB1, we blocked the activity of NLRP3 activity using its specific inhibitor, MCC950. We found that in MCC950-treated BMDMs from *Phb1*^{MyeKO} mice, *Phb1* knockout fails to increase the levels of cleaved IL-1 β in both cytosol and medium (Fig 3M).

Since AIM2, contributing to the activation of AIM2-inflammasome, serves as a double-strand DNA sensor, we also investigated its role in *Phb1* deficiency-related inflammasome

Figure 3. PHB1 knockdown promotes mPTP-dependent mtDNA release.

- A The co-localization between mtDNA (SG-ALK, green) and mitochondria (MitoTracker, red) was examined in J774A.1 cells with or without knockdown of *Phb1* or *Phb2*. White boxed regions in the panels are enlarged. The white arrows indicate mtDNA outside mitochondria. Scale bar: 10 μ m.
- B Quantitative analysis of data from (A). Data are from 10, 8, and 7 images from three independent experiments (left to right, respectively) (mean \pm SEM). n.s., no significance, ****P* < 0.001 (Student's *t*-test).
- C J774A.1 cells with or without *Phb1* knockdown were lysed, and DNA was extracted. qPCR assays were used to detect the mtDNA levels (*D-loop*) in the cytosol relative to nuclear DNA levels (*Tert*) in the whole cell lysates. Data are from six independent experiments (mean \pm SEM). *****P* < 0.0001 (Student's *t*-test).
- D BMDMs isolated from *Phb1*^{Fl/Fl} mice and *Phb1*^{MyeKO} mice were fixed and subjected to IF analysis to detect the co-localization between mitochondria (MitoTracker, red) and mtDNA (SG-ALK, green). White boxed regions in the panels are enlarged. The white arrows indicate mtDNA outside mitochondria. Scale bar: 10 μ m.
- E Quantitative analysis of data from (D). Data are from 10 and 8 images from three independent experiments (mean \pm SEM). ***P* < 0.01 (Student's *t*-test).
- F PBMCs were extracted from *Phb1*^{Fl/Fl} mice and *Phb1*^{MyeKO} mice. Cells were lysed, and DNA was extracted. qPCR assays were used to detect the levels of mtDNA (*D-loop*) in the cytosol relative to the levels of nuclear DNA levels (*Tert*) in the whole cell lysates. Data of PBMC are from seven *Phb1*^{Fl/Fl} mice and *Phb1*^{MyeKO} mice, respectively (mean \pm SEM). ***P* < 0.01 (Student's *t*-test).
- G HeLa cells expressing TFAM-FLAG with or without *Phb1* knockdown were incubated with CsA (2 μ M) for 30 min. Cells were fixed and subjected to IF analysis to detect the co-localization between mitochondria (anti-TOMM20, red) and TFAM-FLAG (anti-FLAG, green). White boxed regions in the panels are enlarged. The white arrows indicate mtDNA outside mitochondria. The yellow arrows indicate mtDNA inside mitochondria. Scale bar: 10 μ m.
- H Quantitative analysis of data from (G). Data from 30, 27, 25, and 24 images from three independent experiments (mean \pm SEM). *****P* < 0.0001 (Student's *t*-test).
- I HeLa cells with or without *Phb1* knockdown were incubated with H₂O₂ (5 mM) for 20 min and CsA (4 μ M) for 12 h. Cells were lysed, and DNA was extracted. qPCR assays were used to detect mtDNA levels (*ND1*) in the cytosol and nuclear DNA levels (*18S*) in the whole cell lysates. Data are from four independent experiments (mean \pm SEM). ***P* < 0.01, *****P* < 0.001, *****P* < 0.0001 (Student's *t*-test).
- J, K HeLa cells with or without *Phb1* knockdown were incubated with VBIT-4 (10 μ M) for 1 h and subsequently lysed, and DNA was extracted. qPCR assays were used to detect mtDNA levels (*ND1* in HeLa cells or *D-loop* in J774A.1 cells) in the cytosol relative to nuclear DNA levels (*TERT* in HeLa cells or *Tert* in J774A.1 cells) in the whole cell lysates. Data are from three independent experiments (mean \pm SEM). n.s., no significance, **P* < 0.05, ***P* < 0.01, *****P* < 0.001 (Student's *t*-test).
- L J774A.1 cells with or without *Phb1* knockdown were lysed. The whole cell lysates were immunoprecipitated by IgG or anti-ASC antibody and the resulting proteins were detected by WB assay.
- M BMDMs isolated from *Phb1*^{Fl/Fl} mice and *Phb1*^{MyeKO} mice were incubated with MCC950 (50 nM) for 30 min and were subsequently stimulated by LPS (200 ng/ml) for 6 h and ATP (4 mM) for 45 min. Protein levels in whole cell lysates and culture medium were detected by WB assay.

Source data are available online for this figure.



activity. Firstly, we did not observe the alteration in AIM2 levels upon the stimulation of poly (dA:dT). Under the *Phb1* deficiency condition, the stimulation of poly (dA:dT) promoted increased production of IL-1 β (Appendix Fig S5A). Subsequently, we asked whether AIM2-inflammasomes are involved in the production of IL-1 β upon inflammatory stresses. We noticed that AIM2 ablation slightly decreased the production of IL-1 β in *Phb1*-depleted cells (Appendix Fig S5B).

The cytosolic mtDNA and ROS promoted by *Phb1*-depletion contribute to the inflammatory responses

Previous studies reported that the cytosolic mtDNA can bind to NLRP3 and is involved in the activation of NLRP3-inflammasomes (Shimada *et al*, 2012; Pan *et al*, 2018; Li *et al*, 2020; Wang *et al*, 2021). To investigate whether the effluxed mtDNA by *Phb1* deficiency is sensed by NLRP3, we firstly examined the co-localization between mtDNA and NLRP3. In physiological conditions, the co-localization between mtDNA and NLRP3 is rarely observed in BMDMs derived from *Phb1^{F/F}* mice or in cultured J774A.1 cells (Fig 4A–D). Upon combined stimulation with LPS and ATP, more mtDNA co-localizes with NLRP3 (Fig 4A–D). The co-localization occurs in *Phb1* knockdown J774A.1 cells or BMDMs from *Phb1^{MyeKO}* mice even in the absence of LPS and is more obvious with LPS alone or combined treatment with LPS and ATP (Fig 4A–D). In addition, we precipitated NLRP3 in BMDMs with an anti-NLRP3 antibody and evaluated the abundance of mtDNA that bound to NLRP3. We found that knockout of *Phb1* increases the enrichment of mtDNA on NLRP3, regardless of physiological conditions or being stimulated by inflammatory stresses of LPS and ATP (Fig 4E).

Also, we investigated whether the other DNA conjugate AIM2 recognizes mtDNA and promotes the production of IL-1 β in *Phb1*-deficient cells. We observed that *Phb1* deficiency fails to increase the co-localization between mtDNA and AIM2, regardless of in physiological conditions or upon inflammatory stimulation of LPS and ATP (Appendix Fig S5C and D). Additionally, we precipitated AIM2 in J774A.1 cells with an anti-AIM2 antibody and detected the abundance of mtDNA binding to AIM2. Although poly (dA:dT) increases the binding between mtDNA and AIM2, *Phb1* deficiency did not promote more enrichment of mtDNA on AIM2 (Appendix Fig S5E).

Subsequently, we generated $\rho 0$ J774A.1 cells by depleting mtDNA in J774A.1 cells with the treatment of EtBr for 3 days as described previously (Nakahira *et al*, 2011; Rongvaux *et al*, 2014; Appendix Fig S6A and B). We found that in $\rho 0$ cells, mtDNA depletion decreased the production of IL-1 β with the stimulation of LPS and ATP. Upon mtDNA depletion, knockdown of *Phb1* fails to elevate the level of cleaved IL-1 β , as compared to normal J774A.1 cells (Fig 4F). These results suggest that the maturation of IL-1 β induced by PHB1 deficit is dependent on mtDNA. Increased intracellular ROS also triggers the activation of NLRP3-inflammasomes (Zhong *et al*, 2016). We found that NAC can decrease the ROS levels in J774A.1 cells (Appendix Fig S6C) and thus inhibit the increased production of IL-1 β induced by *Phb1* deficiency, seemingly with less impact than mtDNA (Fig 4F and G).

The previous studies reported that cytoplasmic exposure of mtDNA also activates the cGAS-STING pathway, which promotes the expression of interferon (IFN) and IFN-stimulated genes (ISGs) (Riley & Tait, 2020). We used BMDMs from *Phb1^{MyeKO}* mice to examine the downstream genes of the cGAS-STING pathway and found that *Phb1* knockout activates the transcription of two ISGs, *Isg15* and *Cxcl10*, in both physiological conditions and the stimulation of H₂O₂, which is considered to induce mtDNA release (Appendix Fig S7A and B).

PHB1 regulates the formation of mPTP by modulating the interaction between SPG7 and AFG3L2

SPG7 binds the mPTP core component CYPD in the mitochondrial matrix and VDAC in the outer mitochondrial membrane. The interaction between SPG7 and AFG3L2 indicates the existence of mPTP (Shanmughapriya *et al*, 2015). Oligomycin Sensitivity-Confering Protein Subunit of ATP synthase (OSCP) has also been reported to bind CYPD (Giorgio *et al*, 2013). Therefore, we first wanted to know whether PHB1 can interact with OSCP, VDAC, SPG7, or AFG3L2. As shown in Appendix Fig S6A, overexpressed PHB1-FLAG precipitates AFG3L2 and SPG7 but not VDAC or OSCP (Appendix Fig S8A). Therefore, we focused on how PHB1 regulates SPG7- and AFG3L2-mediated mPTP opening.

We found that PHB1 strongly interacts with SPG7 and AFG3L2 under normal conditions in HeLa cells (Fig 5A). However, in H₂O₂-

Figure 4. Cytosolic mtDNA and ROS promoted by *Phb1* depletion contribute to the inflammatory responses.

- A BMDMs isolated from *Phb1^{F/F}* mice and *Phb1^{MyeKO}* mice were stimulated with LPS (200 ng/ml) for 6 h, and ATP (4 mM) for 45 min. Cells were fixed and subjected to IF analysis to detect the co-localization between NLRP3 (anti-NLRP3, red) and mtDNA (PicoGreen, green). White boxed regions in the panels are enlarged. The white arrows indicate mtDNA co-localized with NLRP3. Scale bar: 10 μ m.
- B Quantitative analysis of data from (A). Data are from at least 14 images from three independent experiments (mean \pm SEM). **** P < 0.0001 (Student's *t*-test).
- C J774A.1 cells with or without *Phb1* knockdown were stimulated with LPS (200 ng/ml) for 6 h and ATP (4 mM) for 45 min. Cells were fixed and subjected to IF analysis to detect the co-localization between NLRP3 (anti-NLRP3, red) and mtDNA (PicoGreen, green). White boxed regions in the panels are enlarged. The white arrows indicate mtDNA co-localized with NLRP3. Scale bar: 10 μ m.
- D Quantitative analysis of data from (C). Data are from at least six images from three independent experiments (mean \pm SEM). * P < 0.05, ** P < 0.01, **** P < 0.0001 (Student's *t*-test).
- E J774A.1 cells with or without *Phb1* knockdown were stimulated with LPS (200 ng/ml) for 6 h and ATP (4 mM) for 45 min. After cells were lysed, NLRP3 was immunoprecipitated by anti-NLRP3 antibody. mtDNA levels (*D-loop*) from immunoprecipitants were detected by qPCR in J774A.1 cells with or without *Phb1* knockdown. Data are from five independent experiments (mean \pm SEM). ** P < 0.01, **** P < 0.0001 (Student's *t*-test).
- F J774A.1 cells with *Phb1* knockdown were incubated with EtBr (150 ng/ml) for 3 days, followed by LPS (200 ng/ml) for 6 h and ATP (4 mM) for 45 min. WB was used to detect the protein levels in whole cell lysates and culture medium.
- G BMDMs isolated from *Phb1^{F/F}* mice and *Phb1^{MyeKO}* mice were treated with NAC (2 mM) for 8 h, LPS (200 ng/ml) for 6 h and ATP (4 mM) for 45 min. WB assay was used to detect the protein levels in whole cell lysates and in the culture medium.

Source data are available online for this figure.

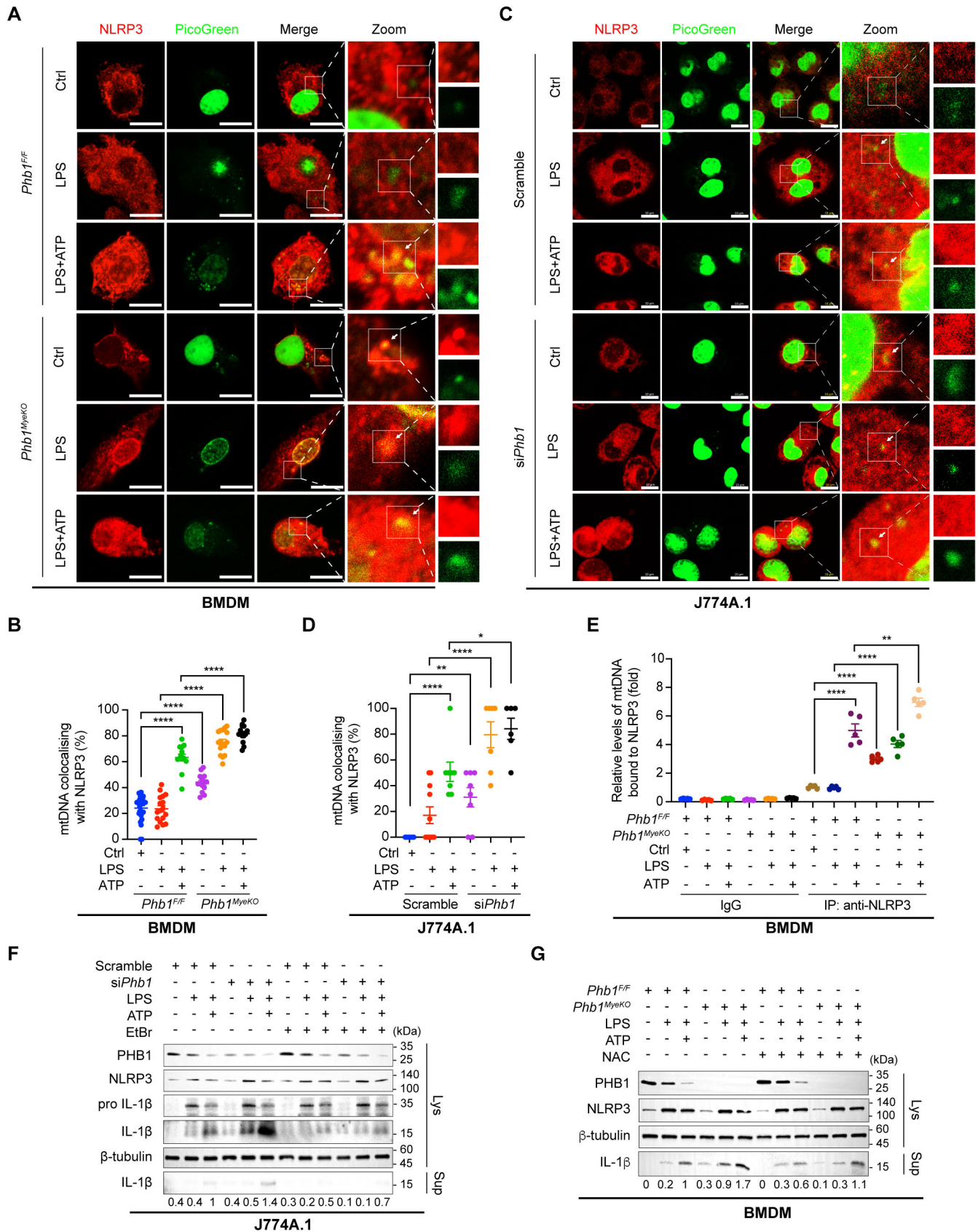


Figure 4.

stimulated HeLa cells, the PHB1 level is reduced and more SPG7 associates with AFG3L2 endogenously (Fig 5A). Accordingly, more endogenous AFG3L2 can be also precipitated by anti-SPG7 antibody (Fig 5A). Consistent with the stimulatory effect of H₂O₂ in nonimmune HeLa cells, LPS treatment also reduces the PHB1 level and enhances the endogenous interaction between SPG7 and AFG3L2 in J774A.1 cells (Fig 5B).

Similar to the effect of H₂O₂ or LPS, both of which open mPTP, the knockdown of *Phb1* itself significantly enhances the interaction between endogenous SPG7 and AFG3L2 in both HeLa cells and J774A.1 cells (Fig 5C and D).

SPG7 and AFG3L2 are both required for mtDNA release and inflammation activation mediated by PHB1 deficiency

Above, we showed that mPTP opening and mtDNA release induced by PHB1 deficiency is VDAC- and CYPD-dependent. Shanmughapriya

et al revealed that SPG7, as a core component of mPTP, interacts with VDAC and CYPD to promote the opening of mPTP. Additionally, SPG7 binds AFG3L2 to form the *m*-AAA protease complex, which is regulated by PHB1 (Shanmughapriya *et al*, 2015). Thus, we asked whether SPG7 and AFG3L2 are involved in mtDNA release and inflammation activation induced by oxidative stress, LPS, or *Phb1* knockdown.

Upon treatment of *Phb1* KD HeLa cells with H₂O₂, the levels of SPG7 and AFG3L2 remain stable (Fig 5A; Appendix Fig S9A). This indicates that SPG7 and AFG3L2 do not depend on their altered expression to participate in the opening of mPTP. Additionally, in *Phb1* KD HeLa cells, the disorder in mitochondrial Ca²⁺ uptake is recovered by additional knockdown of SPG7 or AFG3L2 (Appendix Fig S9B–E). We found that the co-localization between mtDNA and mitochondria is reduced in *Phb1*-depleted J774A.1 cells or HeLa cells, whereas additional knockdown of SPG7 or AFG3L2 restores the co-localization (Fig 6A and B; Appendix Fig S9F).

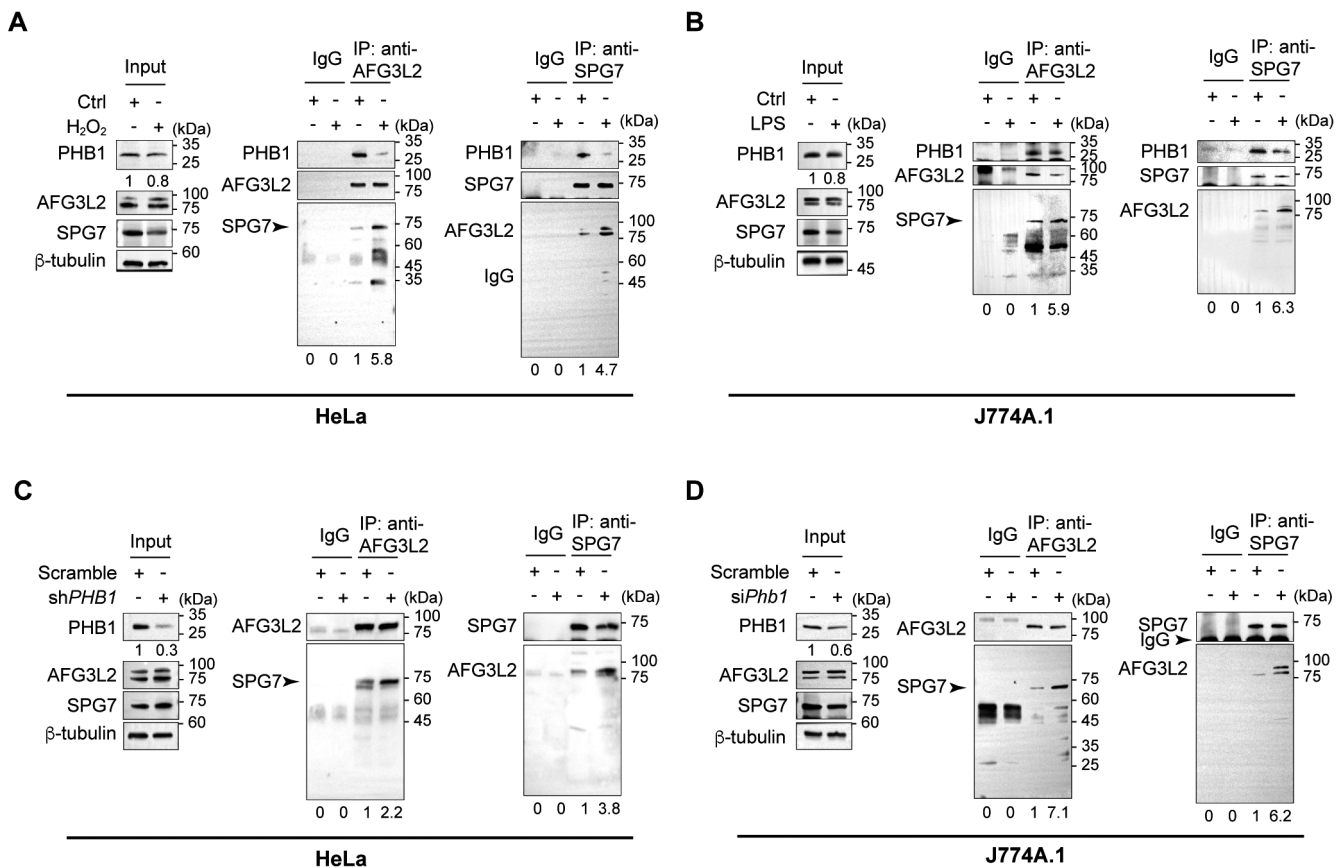


Figure 5. PHB1 regulates the formation of mPTP by modulating the interaction between SPG7 and AFG3L2.

- A HeLa cells were incubated with H₂O₂ (5 mM) for 20 min and then lysed. The whole cell lysate was immunoprecipitated by IgG, anti-AFG3L2 antibody, or anti-SPG7 antibody. WB was used to detect the SPG7 or AFG3L2 levels, respectively, in the precipitated products.
- B J774A.1 cells were stimulated with LPS (200 ng/ml) for 6 h and lysed. The whole cell lysate was immunoprecipitated by IgG, anti-AFG3L2 antibody, or anti-SPG7 antibody. The respective levels of precipitated SPG7 or AFG3L2 were examined by WB.
- C, D HeLa cells or J774A.1 cells with or without *Phb1* knockdown were lysed. The whole cell lysate was immunoprecipitated by IgG, anti-AFG3L2 antibody, or anti-SPG7 antibody. The respective levels of precipitated SPG7 or AFG3L2 were examined by WB.

Source data are available online for this figure.

Subsequently, we verified that synergistically knocking down PHB1/SPG7 or PHB1/AFG3L2 suppresses the cytoplasmic mtDNA level, which is increased by knockdown of PHB1 alone (Fig 6C).

Additionally, the increased production of cleaved IL-1 β induced by PHB1 knockdown is repressed with additional knockdown of SPG7 or AFG3L2 (Fig 6D-F).

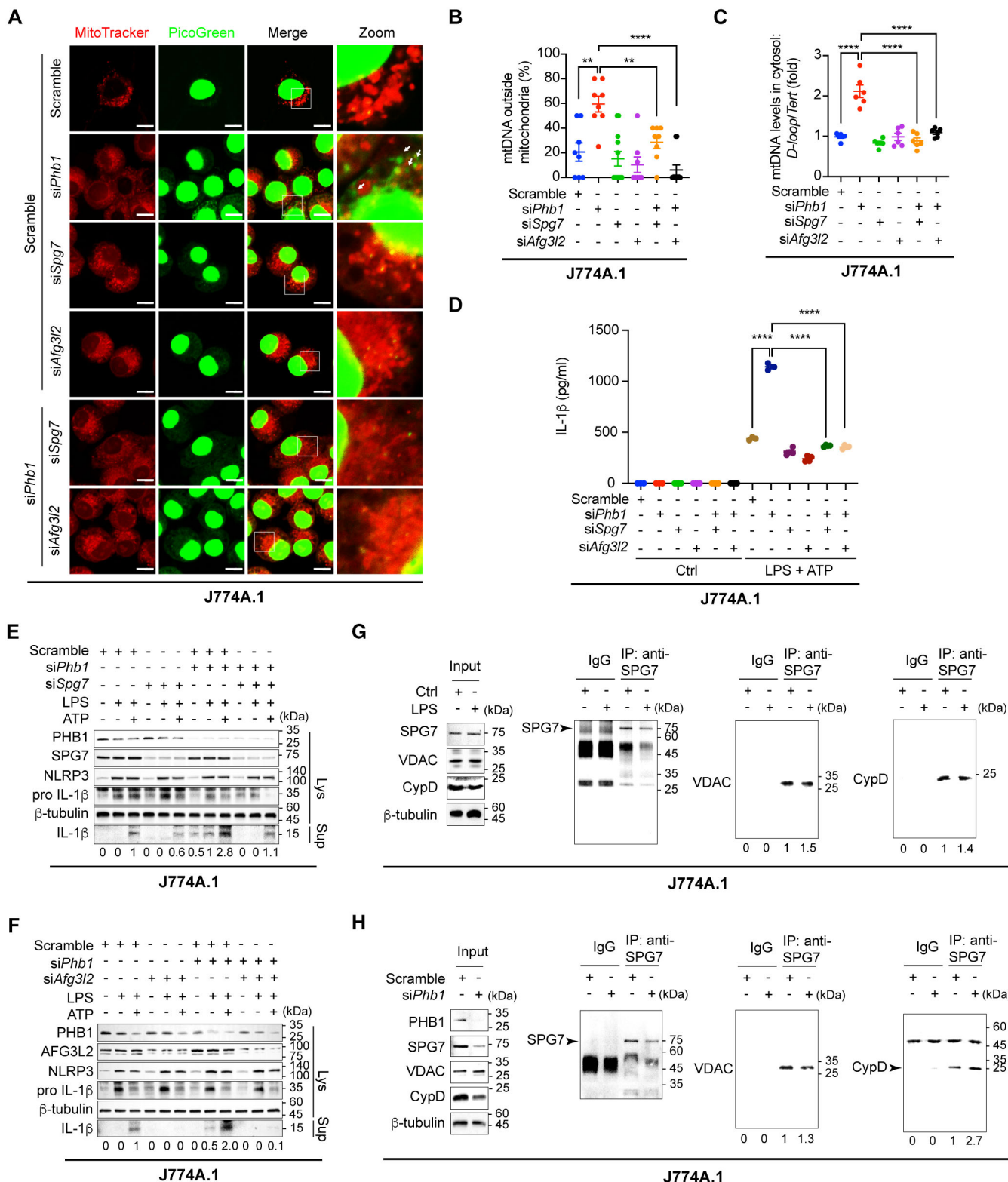


Figure 6.

Figure 6. SPG7 and AFG3L2 are both required for mtDNA release and inflammatory responses mediated by *Phb1* knockdown.

- A J774A.1 cells with knockdown of *Phb1* alone, *Afg3l2* alone, *Spg7* alone, *Phb1* + *Afg3l2*, or *Phb1* + *Spg7* were fixed and subjected to IF analysis to assess the colocalization between mitochondria (MitoTracker, red) and mtDNA (PicoGreen, green). White boxed regions in the panels are enlarged. The white arrows indicate mtDNA outside mitochondria. Scale bar: 10 μ m.
- B Quantitative analysis of the data from (A). Data are from at least 12 images from three independent experiments (mean \pm SEM). ** P < 0.01, **** P < 0.0001 (Student's t -test).
- C J774A.1 cells with knockdown of *Phb1* alone, *Afg3l2* alone, *Spg7* alone, *Phb1* + *Afg3l2*, or *Phb1* + *Spg7* were lysed, and DNA was extracted. qPCR was used to detect the mtDNA levels (*D-loop*) in the cytosol relative to the nuclear DNA levels (*Tert*) in the whole cell lysate. Data are from six independent experiments (mean \pm SEM). **** P < 0.0001 (Student's t -test).
- D J774A.1 cells with knockdown of *Phb1* alone, *Afg3l2* alone, *Spg7* alone, *Phb1* + *Afg3l2*, or *Phb1* + *Spg7* were stimulated with LPS (200 ng/ml) for 6 h and ATP (4 mM) for 45 min. The culture medium was collected and ELISA assays were used to detect IL-1 β levels in the culture medium. Data are from four independent experiments (mean \pm SEM). **** P < 0.0001 (Student's t -test).
- E J774A.1 cells with *Phb1* knockdown, *Spg7* knockdown, or combined *Phb1* and *Spg7* knockdowns were stimulated with LPS (200 ng/ml) for 6 h and ATP (4 mM) for 45 min. WB assay was used to detect the protein levels in whole cell lysates and culture medium.
- F J774A.1 cells with *Phb1* knockdown, *Afg3l2* knockdown, and combined *Phb1* and *Afg3l2* knockdowns were stimulated with LPS (200 ng/ml) for 6 h and ATP (4 mM) for 45 min. WB assay was used to detect the protein levels in whole cell lysates and culture medium.
- G J774A.1 cells were stimulated with LPS (200 ng/ml) for 6 h and lysed. The whole cell lysate was immunoprecipitated by IgG or anti-SPG7 antibody. WB was used to detect the CYPD and VDAC levels in the precipitated products.
- H J774A.1 cells with or without *Phb1* knockdown were lysed. The whole cell lysates were immunoprecipitated by IgG or anti-SPG7 antibody. WB was used to detect the CYPD and VDAC levels in the precipitated products.

Source data are available online for this figure.

The interaction of SPG7 with VDAC or with CYPD is not influenced by PHB knockdown

SPG7/VDAC or SPG7/CYPD interaction mediates the opening of mPTP as evidenced by a previous study (Shanmughapriya *et al*, 2015). Therefore, we examined whether the interaction between SPG7/VDAC and SPG7/CYPD will be altered under conditions of inflammation or *Phb1* knockdown. Under each condition, we failed to see an altered interaction between SPG7/VDAC and SPG7/CYPD in J774A.1 cells (Fig 6F–H). These results suggest that the opening of mPTP is not determined by alterations in the interactions between SPG7, VDAC, and CYPD, or by changes in the levels of these proteins.

Discussion

Recently, evidence has accumulated that mtDNA is important for the initiation of sterile innate immune responses (Riley & Tait, 2020). The channels that allow mtDNA to cross through the outer mitochondrial membrane have been extensively studied (McArthur *et al*, 2018; Kim *et al*, 2019). For instance, it has been reported that BAX and BAK are recruited to the outer mitochondrial membrane where they form macropores, followed by cytochrome C release and inner mitochondrial membrane herniation prior to the release of mtDNA and activation of the cGAS-STING pathway (McArthur *et al*, 2018; Riley *et al*, 2018). The authors claimed that, during this extreme event, the manner in which mtDNA passes through the inner mitochondrial membrane is independent of the opening of mPTP.

Evidence from another group has demonstrated that during oxidative stress, mtDNA is released through macropores formed by oligomerization of VDACs and thus encounters the DNA sensor cGAS, which leads to TBK1 phosphorylation and IFN production (Kim *et al*, 2019). The authors proposed that the opening of mPTP induces mitochondrial inner membrane instability and mtDNA release (Kim *et al*, 2019). Yu *et al* (2020) showed that mtDNA

passes through both mitochondrial membranes via mPTP in amyotrophic lateral sclerosis (ALS). Although the authors provided different mechanisms by which mtDNA escapes from the outer mitochondrial membrane, these studies failed to clarify how mtDNA passes through the inner mitochondrial membrane, nor did they identify which factors play key roles in MIMP by regulating mPTP opening.

More notably, although mPTP is involved in VDAC-dependent mtDNA release induced by oxidative stress and pro-inflammatory conditions (Kim *et al*, 2019; Yu *et al*, 2020), it does not appear to be involved in BAX/BAK-dependent mtDNA release induced by proapoptotic conditions (McArthur *et al*, 2018; Riley *et al*, 2018). Also, VDAC-mPTP channels can only release mtDNA fragments of about 110 bp, whereas the opening of BAX/BAK macropores can cause inner mitochondrial membrane herniation and nucleoid release into the cytoplasm (McArthur *et al*, 2018; Kim *et al*, 2019). Therefore, further work is required to determine whether different stress conditions can induce different molecularly mediated MIMPs and whether various forms of MIMPs can mediate the efflux of different sizes of mtDNA.

The current evidence showed there were different insights in the specific sensor to recognize mtDNA and mediate the downstream pathways. Although NLRP3, recognizing PAMPs and DAMPs, seems to sense oxidized mtDNA and lead to the activation of NLRP3-inflammasomes (Shimada *et al*, 2012; Pan *et al*, 2018; Li *et al*, 2020; Wang *et al*, 2021), whether mtDNA directly triggers this event remains controversial (Holley & Schroder, 2020; Riley & Tait, 2020). Nevertheless, other factors involving defects in mitochondrial function (including loss of membrane potential, increased ROS, or perturbations in mitochondrial electron transport chain) are also associated with inflammasome activation (Zhou *et al*, 2011; Zhong *et al*, 2016; Billingham *et al*, 2022). Additionally, other sensors represented by cGAS and AIM2 can directly recognize mtDNA with their specific DNA-binding domain and activate IFN-related pathways (Kim *et al*, 2019; Yu *et al*, 2020) and AIM2-inflammasomes (Wang *et al*, 2021), respectively. Recently, Xian *et al* (2022) found that upon the stimulations of NLRP3 activators, ox-mtDNA reaches

the cytosol via mPTP- and VDAC- dependent channels and activates NLRP3-inflammasomes and cGAS-STING pathways. However, the results from our laboratory (not shown) and other laboratories show the limitations of using 8-OH-dG to stain ox-mtDNA. They are not very specific and the fluorescence of ox-mtDNA shows a diffuse distribution, which could be related to the principle of the method itself, in which all oxidized DNA in the cell is stained, causing a large amount of background fluorescence. A more convincing method to solve this difficulty remains to be developed in this field (Zhong et al, 2018; Shu et al, 2021). In the present study, we did confirm that mtDNA releases and is involved in these pathways above and found that *Phb1* deficiency-dependent mtDNA release may be associated with the activation of both NLRP3-inflammasomes and cGAS-STING pathways. Meanwhile, we also found that *Phb1* deficiency-dependent high ROS levels get involved in NLRP3-inflammasomes activation. Thus, PHB1 may regulate inflammatory responses via multiple effects on mitochondrial functions.

EtBr is widely used to generate $\rho 0$ cell lines with low mtDNA levels for investigation of the roles of mtDNA in inflammasomes

and cGAS-STING axis (Yu et al, 2020; Wang et al, 2021). EtBr treatment also has profound effects on cellular homeostasis, including increased intracellular ROS level, glycolysis, and reduced autophagic level (Nacarelli et al, 2014; Warren et al, 2017). Of note, increased ROS level and glycolysis as well as reduced autophagic level promote the activation of NLRP3-inflammasome (Zhou et al, 2011; Xie et al, 2016; Zhong et al, 2016), whereas lower mtDNA level blocks NLRP3-inflammasomes activation (Zhong et al, 2016). Consistent with the previous studies (Zhong et al, 2016; Wang et al, 2021), we also generated the $\rho 0$ J774A.1 cells and found that mtDNA depletion blocks the activation of inflammasomes. Thus, we believe that methodology should be further improved for investigating the roles of mtDNA in the activation of inflammasomes and cGAS-STING pathways.

Under these circumstances, we paid more attention to the mechanisms of MIMP during inflammatory responses and investigated what factors regulate MIMP, leading to mtDNA crossing the inner mitochondrial membrane into the cytosol in the present study. We propose that the release of mtDNA from the mitochondrial matrix

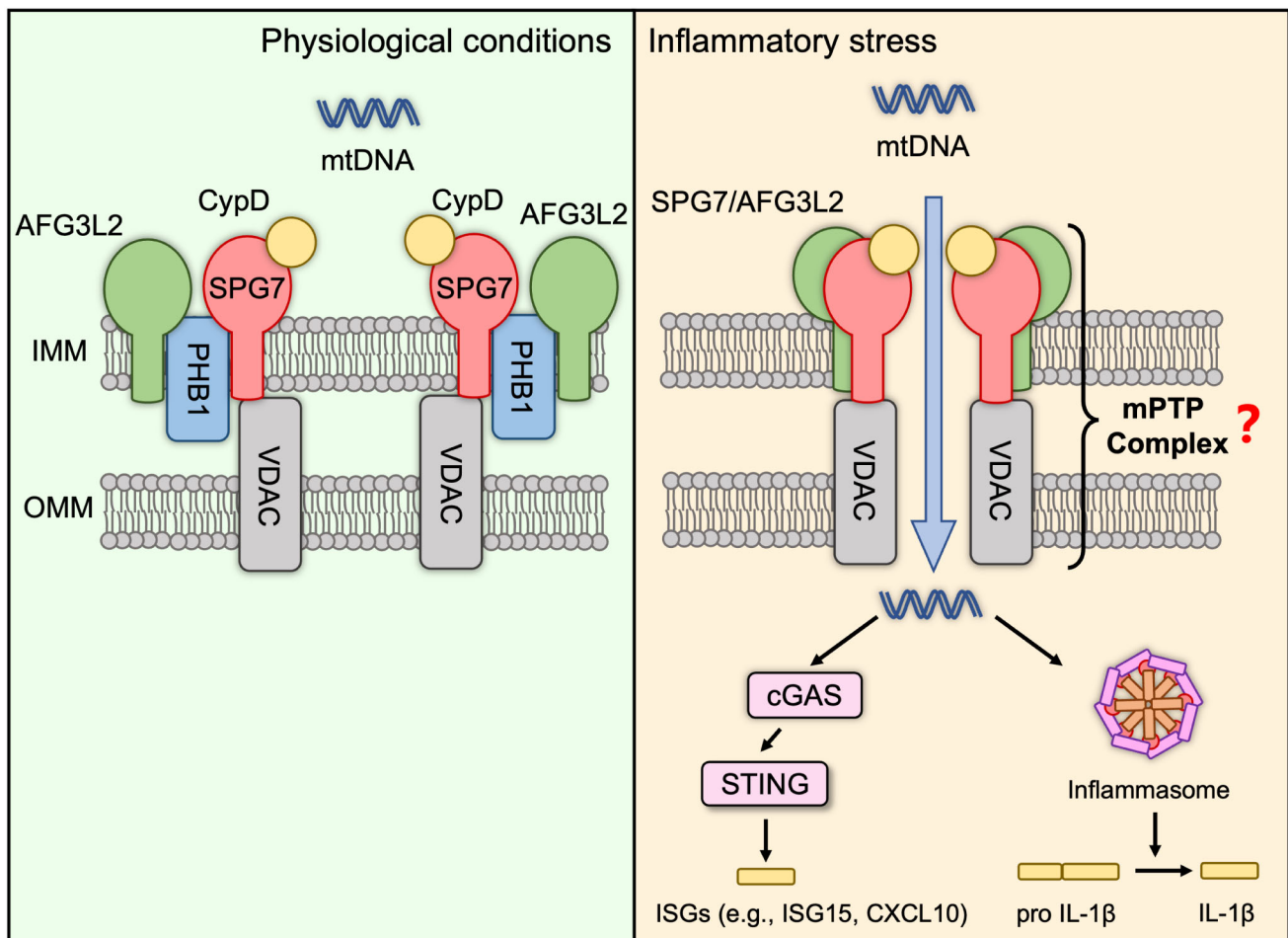


Figure 7. Proposed working model of the role of PHB1 under normal and inflammatory stress conditions.

Under normal physiological conditions, two inner membrane resident proteins, AFG3L2 and SPG7, are tethered to PHB1. The mitochondrial permeability transition pore (mPTP) is inactive and mtDNA is retained in the matrix. In cells under inflammatory stress (e.g., induced by LPS), or in cells with PHB1 knockdown, the interaction between AFG3L2 and SPG7 is significantly enhanced, which promotes the formation of mPTP. This leads to mtDNA release and downstream inflammatory responses.

firstly requires contact with inner mitochondrial membrane proteins or lipids and then transport across the inner and outer membranes. PHB1 emerged in our search for mtDNA-interacting proteins located in the inner mitochondrial membrane. We think it could be a perfect candidate because it can regulate GEP1 and USP1 to maintain the levels of cardiolipin and phosphatidylethanolamine (PE) in the inner mitochondrial membrane (Osman *et al*, 2009). PHB1 assists its binding partner MDM33 to maintain cardiolipin and PE levels in the inner mitochondrial membrane (Klecker *et al*, 2015). Thus, PHB1 has been considered to be an essential scaffold in the mitochondrial inner membrane. More importantly, the association between PHB1 and mtDNA was found several years ago. Kasashima *et al* (2008) identified that PHB1 is a mitochondrial nucleoid component and maintains the copy number of mtDNA. Therefore, PHB1 is very likely to be a critical protein for mtDNA efflux.

There are vigorous debates regarding the composition of mPTP. Shanmughapriya *et al* demonstrated that SPG7 is a core component of mPTP and interacts with VDAC1 and CYPD. They also showed that SPG7 knockdown impairs the mitochondrial calcium retention capacity (Shanmughapriya *et al*, 2015). By contrast, Bernardi and Forte (2015, 2016) proposed that SPG7 is an indirect regulator of mPTP opening and MIMP rather than a core component of mPTP. In the last decade, some evidence suggests that mPTP is formed by the rearrangement of ATP synthase (Giorgio *et al*, 2013). Therefore, the exact mechanism underlying mPTP formation is still controversial, and it is possible that the composition of mPTP may differ under diverse stimulation conditions.

Our study identified that PHB1, a core factor in the inner mitochondrial membrane, controls mPTP formation and MIMP by regulating the interactions between SPG7 and AFG3L2. Specifically, under normal conditions, two inner membrane resident proteins, AFG3L2 and SPG7, are tethered to PHB1. However, under oxidative stress- or LPS-induced mPTP opening conditions, or in cells with *Phb1* knockdown, the binding between AFG3L2 and SPG7 is significantly reinforced, thus promoting the formation of mPTP. Although genetic deficiency of CYPD seems to have no effect on inflammatory responses (Allam *et al*, 2014), the loss of another potential mPTP regulator, SPG7, did block the activation of NLRP3-inflammasomes in our study. In this way, mtDNA is exposed to the cytosol and activates downstream inflammatory responses (Fig 7).

The present study also provides evidence of an anti-inflammatory role for PHB1 in sepsis, consistent with the previous study (Guo *et al*, 2020). During T-cell activation, PHB1 expression at the plasma membrane is upregulated (Yurugi *et al*, 2012; Buehler *et al*, 2018). In LPS-induced acute lung injury, the PHB1 level is also increased in alveolar epithelial cells (Zhang *et al*, 2018). By contrast, more studies have shown that LPS stimulation downregulates the PHB1 level in epithelial cells and that overexpression of PHB1 alleviates inflammation and restores body weight (Theiss *et al*, 2009, 2011). Unfortunately, these studies failed to reveal the mechanism by which PHB1 regulates inflammation, whereas our study found that the downregulation of PHB1 in response to LPS stimulation promotes the formation of mtDNA-dependent inflammasomes, which may lead to the progression of sepsis. We also noticed that IL-1 β levels were around 100 pg/ml in *Phb1*^{F/F} mice without LPS treatment, which may lead to inflammatory status, but the previous studies also showed similar levels in the control group (Zhong *et al*, 2016; Chen *et al*, 2020). Although some individuals had higher basal

inflammation, any of their behavioral manifestations were normal. Collectively, our results reveal novel mechanistic roles of PHB1 not only in the initiation of innate immunity but also in the downstream responses.

Materials and Methods

Mice

LysM-Cre mice were obtained from Yiming Xu's Lab, Guangzhou Medical University, China. *Phb1*^{F/F} mice were generated by Biocytogen Pharmaceuticals Co., Ltd (Beijing, China). *LysM-Cre* mice were crossed with *Phb1*^{F/F} mice to generate *Phb1*^{MyeKO} mice. *Phb1*^{F/F} littermates were used as controls in all assays in this study. Whole body *Phb1*^{+/-} mice were generated by Biocytogen Pharmaceuticals Co., Ltd (Beijing, China). The drug administration of animals was according to the blind strategy. All mice were bred in the eligible animal housing facility at Guangzhou Medical University according to the guidelines of the Institutional Animal Care and Use Committee of UCSD (ID: GY2019-017).

Reagents and antibodies

LPS (*E. coli* O111:B4) were from Sigma-Aldrich (L2630). ATP was from Sigma-Aldrich (A7699). Histamine was from Solarbio (H8240). Cyclosporin A was from Solarbio (C8780). FCCP was from Meilunbio (MB3642). VBIT-4 was from Selleck Chemicals (S3544). Oligomycin was from Meilunbio (MB5431). Antimycin A was from Enzo Life Sciences (ALX-380-075). Rotenone was from Sigma-Aldrich (R8875). Ethidium Bromide was Sigma-Aldrich (E7637). Puromycin was from Sigma-Aldrich (P8833). TMRM was from Anaspec (AS-88065). DHE was from US EVERBRIGH (D1008). MCC950 was from MCE (HY-12815A). H₂O₂ was from Huankai Microbial (029161). DMSO was from Solarbio (D8371). SG-ALK was obtained from Shoufa Han's Lab, Xiamen University. MitoTracker™ Red CMXRos was from Invitrogen (M7512). Quant-iT™ PicoGreen™ dsDNA Reagent was from Invitrogen (P11495). Transfection was performed with Hieff Trans™ Liposomal Transfection Reagent (YEASEN, 40802ES02) or Lipofectamine™ 2000 Transfection Reagent (Invitrogen, 11668019). ELISA assays were performed with Mouse IL-1 beta ELISA Kit (Proteintech Group, KE10003). Antibodies for co-immunoprecipitation assays, Western blotting assays or immunofluorescence analysis were: anti-Prohibitin/PHB1 (ab75766, Abcam; MAB10296, Abnova; 10787, Proteintech Group), anti-PHB2 (14085, Cell Signaling Technology), anti-NLRP3 (15101, Cell Signaling Technology, AG-20B-0014, Adipogen), anti-ASC (67824, Cell Signaling Technology), anti-IL-1 β (12426/12242, Cell Signaling Technology), anti-AFG3L2 (14631-1-AP, Proteintech Group), anti-paraplegin/SPG7 (sc-514393, Santa-Cruz), anti-VDAC (4661S, Cell Signaling Technology), anti-CypD (18466-1-AP, Proteintech Group), anti-OSCP (sc-365162, Santa-Cruz), anti-Caspase-1 (24232S, Cell Signaling Technology), anti-AIM2 (66902-1-IG, Proteintech Group), anti-TOMM20 (11802-1-AP, Proteintech Group), anti-FLAG (66008-3-Ig/80010-1-RR, Proteintech Group), anti-HA (3724S, Cell Signaling Technology), anti-GAPDH (60004-1-Ig, Proteintech Group), anti- β -tubulin (10068-1-AP, Proteintech Group), anti-DNA (AC-30-10, Progen), HRP-conjugated Affinipure Goat Anti-Mouse IgG(H + L)

(SA00001-1, Proteintech Group), HRP-conjugated Affinipure Goat Anti-Rabbit IgG(H + L) (SA00001-2, Proteintech Group), Alexa Fluor 488 goat anti-Rabbit (A11008, Invitrogen), Alexa Fluor 594 goat anti-Rabbit (A11037, Invitrogen), Alexa Fluor 488 goat anti-Mouse (A32723, Invitrogen), Alexa Fluor 594 donkey anti-Mouse (A21203, Invitrogen), Mouse IgG (3420, Cell signaling technology), Rabbit IgG (2729, Cell signaling technology). RIPA lysis was from SAB (SA7951). The protease inhibitor cocktail was from Beyotime (P1006); PMSF (Phenylmethanesulfonyl fluoride) was from Beyotime (ST505).

Cell culture and infections

HeLa cell line and 293T-cell line were obtained from the National Collection of Authenticated Cell Cultures. J774A.1 cell line was obtained from Kunming Cell Bank. CAS. Primary bone marrow-derived macrophages (BMDM) were obtained from gene-modified mice. As the previous study described (Hornung et al, 2008), after being extracted from the bone marrow, marrow cells were stimulated by 20% vol/vol L929 cultural medium for 7 days to differentiate into macrophages. HeLa cells and 293T cells were cultured in Dulbecco's Modified Eagle Medium (DMEM; Thermo Fisher, 12800-017) supplemented with 10% (v:v) fetal bovine serum (FS301-02, TRANS) at 37°C with 5% (v:v) CO₂. J774A.1 cells and BMDM were cultured in DMEM with 15% (v:v) fetal bovine serum (FS301-02, TRANS) at 37°C with 5% (v:v) CO₂. ShPHB1, 4mt-RCaMPh, or scrambled sequences in lentiviral PLKO.1-puro plasmid were transfected in 293T cells, and the lentivirus was packed. HeLa cells were infected by collected lentivirus containing target sequences. Monoclonal cell lines were selected and maintained by 3 µg/ml puromycin. Cell lines were recently authenticated by STR profiling and tested for mycoplasma contamination.

Isolation of peripheral blood mononuclear cells (PBMCs)

Peripheral venous blood of patients with neonatal septicemia and an equal number of normal controls were collected from The Second Affiliation Hospital of Guangzhou Medical University ($n = 6$, respectively) were collected from PBMCs were extracted with Human PBMCs separation kit (P8670, Solarbio). Institutional review board approval and ethics committee approval were granted for this study and informed consent was signed by the statutory guardian of patients before samples were collected. The collection of peripheral venous blood and extraction of PBMCs were according to the blind strategy. According to the manufacturer's instructions, 5 ml of peripheral venous blood was obtained in tubes with EDTA. Blood was slowly layered on 5 ml Ficoll-Hypaque, followed by the centrifuge at 800 g for 35 min at room temperature (RT) with slow acceleration and deceleration. The buffy coat in gradient was collected and mixed with PBS to 8 ml, followed by the centrifuge at 400 g for 10 min at RT. The pellet was suspended with Red blood cell lysis buffer and incubated for 10 min at 4°C. Washed with PBS, cells were collected in 1.5 ml EP centrifuge tubes for further assays.

Plasmid constructs and transfection

4mt-RcaMPh plasmid was a gift from Xin Pan's Lab, National Center of Biomedical Analysis, China. According to our previous study (Hu

et al, 2021), For other plasmids, target cDNA with the homologous sequence was amplified with Golden Star T6 PCR Super Mix (TSE101, Tsingke). Expression plasmids were digested by restriction enzymes (Takara). Target cDNA was cloned into a digested vector with homologous recombination by Hieff Clone® Plus One Step Cloning Kit (10911ES20, YEASEN). ASC gene was cloned into pCMV expression vectors with HA tag. ASC gene, NLRP3 gene, TFAM gene, and PHB1 gene were cloned into pCMV expression vector with FLAG tag.

The primers were provided as follows:

ASC: 5'-CGCTCTAGCCCGGGCGGATCCATGGGGCGCGCGCGACG
CCAT-3' (Forward), 5'-GTATGGGTATCTAGACTCGAGGCTCCGCTC
CAGGTCCTCCACCA-3' (Reverse)

NLRP3: 5'-GGGAATTCGTCGACTGGATCCATGAAGATGGCAAGCAC
CCGCTGCAAG-3' (Forward), 5'-TGAGATGAGTTTCTGCTCGAGCCA
AGAAGGCTCAAAGACGACGGTCAGC-3' (Reverse)

TFAM: 5'-GGGAATTCGTCGACTGGATCCATGGCGTTTCTCCGAAGC
ATGT-3' (Forward), 5'-TGAGATGAGTTTCTGCTCGAGACACTCCTC
AGCACCATATTTTCG-3' (Reverse)

PHB1: 5'-TACCGAGGAGATCTGCCGCCGCGATCGCCATGGCTGCCA
A-3' (Forward); 5'-CCGCGTACGCGTCTGGGGCAGCTGGAGGAGC
ACGGACTGC-3' (Reverse)

PHB1 shRNAs, SPG7 shRNAs, and scramble control shRNAs were inserted into GV248 vectors (Shanghai GeneChem Co., Ltd; Tsingke Biotechnology Co., Ltd.). The shRNA target sequences were provided as follows:

Scramble: 5'-TTCTCCGAACGTGTCTACGT-3'

PHB1: 5'-AGTGTGAGTCCATTGGCAA-3'

SPG7: 5'-AATGCCTACGTTAAGCTATAC-3'

AFG3L2: 5'-GCTAGAGTCCGAGACTTATTT-3'

Expression plasmids and shRNA were transfected into cells for 36–48 h according to the manufacturer's instructions of transfection reagents, followed by harvest for Western blotting, RT-qPCR, and immunofluorescence analysis.

Transient transfection with siRNA

PHB1, PHB2, SPG7, or AFG3L2 were knocked down by siRNA that was designed and synthesized by Kidan Biosciences co., Ltd (Guangzhou, China).

The sequences were provided as follows:

Scramble: 5'-UUCUCCGAACGUGUCACGUTT-3' (sense), 5'-ACGUGA
CAGGUUCGGAGAATT-3' (antisense)

Phb1: 5'-CGUCAUAUACACACUGCGAAUUTT-3' (sense), 5'-AUUCGC
AGUGUGAUUUGACGTT-3' (antisense)

Phb2: 5'-GCCUCAUUAAGGGUAAGAAUUTT-3' (sense), 5'-AUUUCU
UACCCUUAUGAGGCTT-3' (antisense)

Spg7: 5'-GCAUGUCUUAUUGAUUUUTT-3' (sense), 5'-AAGAUA
AUGAAGACAUGCCCT-3' (antisense)

Afg3l2: 5'-UGUUGCCCACCGUACUCAUUATT-3' (sense), 5'-UUAUG
AGUACGGUGGGCAACATT-3' (antisense)

Aim2: 5'-GGAAGCCAUCAGAGAAGAUUTT-3' (sense), 5'-AUCUUCUC
UGAUGGCUUCCTG-3' (antisense)

Transfection was performed with Hieff TransTM Liposomal Transfection Reagent or LipofectamineTM 2000 Transfection Reagent according to the manufacturer's instructions. The efficiency of knockdown was verified by RT-qPCR and Western blotting assays.

Enzyme-linked immunosorbent assay (ELISA)

ELISA kits were used to detect mouse IL-1 β levels in mice serum (dilution, 1:200) and culture medium according to the manufacturer's instructions.

Western blotting

According to our previous study, we performed the WB assays (Hu et al, 2021). Cells were harvested and lysed by RIPA lysis buffer (RIPA lysis: cocktail: PMSF = 100:1:1). Following centrifuge at 16,215 g for 20 min at 4°C, the supernatant was collected, and the concentration of total proteins was detected by bicinchoninic acid (BCA) kit (23227, ThermoFisher Scientific). All samples were normalized and boiled at 100°C for 10 min. Samples and Protein Marker (20352ES76, YEASEN) were separated by SDS-PAGE with Genshare CFAS any KD PAGE (Genshare Biological), then transferred to PVDF membrane. Membranes carrying samples proteins were blocked by 5% BSA (Bovine Serum Albumin, 4240GR100, BioFroxx) or fat-free milk for 1 h at RT and then were incubated with primary antibodies overnight at 4°C. After being washed by TBST buffer 4 times for 10 min, membranes were incubated with secondary antibodies for 1 h at RT. Subsequently, following washing by TBST buffer 4 times for 10 min, the blots were detected with High-sig ECL Western Blotting Substrate (180-5001, Tanon) and GelView 6000 Pro (Biolight, China).

Co-immunoprecipitation

According to our previous study, we performed the co-immunoprecipitation assays (Hu et al, 2021). For direct co-IP for intracellular proteins, cells were seeded at 10 cm dishes and were harvested at the confluent degree of 80–90%. Cells were lysed with NP-40 lysis buffer (P0013F, Beyotime) for 1 h, and the lysates were centrifuged at 16,215 g for 20 min at 4°C. The supernatant was collected, and the concentration of total proteins was detected by BCA kit. Moved 3,000 μ g proteins into a fresh 1.5 ml EP centrifuge tube, and then added target antibody into the tube, followed by incubation for 12 h at 4°C. Subsequently, for immunoprecipitation, PureProteomeTM Protein A/G Mix Magnetic Beads (LSKMAGAG10, Millipore) or Protein A + G Agaroses (P2055, Beyotime) were pre-washed by PBST (PBS with 0.5% Tween) 3 times and were added into this tube and incubated for 3 h (agaroses for 10 h). Beads were washed by RIPA lysis buffer (Tris 10 mM, NaCl 150 mM, NP-40 1%, SDS 0.1%, deoxycholate 0.1%, pH 7.4) 5 times on ice. All samples were boiled for 10 min.

Immunofluorescence and confocal microscope analysis

According to our previous study, we performed the IF analysis (Hu et al, 2021). For IF analysis, cells were seeded at 12-well plates that contained glass slides overnight. Subsequently, after were stimulated with LPS 200 ng/ml for 6 h and ATP 4 mM for 45 min, cells were fixed with 4% paraformaldehyde (CF189021, Solarbio) for

10 min, and permeabilized in Immunostaining Permeabilization Buffer with Triton X-100 (P0096, Beyotime) for 10 min at RT. Following blocking with QuickBlockTM Blocking Buffer (P0260, Beyotime) for 15 min at RT, cells were incubated with primary antibodies diluted in QuickBlockTM Primary Antibody Dilution Buffer (P0262, Beyotime) at 4°C overnight. After being washed by PBS, cells were incubated with Alexa Fluor secondary fluorescent antibodies for 1 h at RT and then were stained by DAPI.

For detection of DNA or mitochondria, cells were seeded at 12-well plates that contained glass slides overnight. After being stimulated with LPS 200 ng/ml for 6 h and ATP 4 mM for 45 min, cells were incubated with PicoGreen for 1 h, SG-ALK for 30 min, or MitoTracker for 30 min at 37°C. Subsequently, cells were fixed and stained by DAPI.

Images of cells were acquired by LSM 800 META (Carl Zeiss, Germany) or SP8 confocal microscope (Leica, Germany). The analyses of images were performed by Image J 1.53c (National Institutes of Health, USA).

For time-series acquisition of images, cells that stably expressed *4mt-RCaMP* were seeded on dishes with glass walls. Before image acquisition, the culture medium was changed to phenol red-free DMEM with 10% FBS. Before images were acquired, cells were incubated with CsA 2 μ M for 30 min or H₂O₂ 1 mM for 30 min. During a series of image acquisition (interval: 10 s), cells were stimulated with histamine 200 μ M.

Images of time series were acquired by LSM 800 META (Carl Zeiss, Germany). The analyses of images were performed by Image J 1.53c (National Institutes of Health, USA). F₀ indicated the initial fluorescence intensity, while F indicated the fluorescence intensity at each time point. The plots of mitochondrial Ca²⁺ levels were indicated with F/F₀.

Measurement of mitochondrial membrane potential

For measurement of $\Delta\Psi$ m, following treatment with FCCP 4 μ M for 5 min and CsA 2 μ M for 30 min, the cells were incubated with 150 nM TMRM for 30 min at 37°C. Subsequently, cells were resuspended with PBS, and $\Delta\Psi$ m was detected by SP8 confocal microscope (Leica, Germany) and CytoFLEX S (Beckman Coulter Life Sciences, USA).

Measurement of reactive oxidative species (ROS)

For measurement of ROS, following treatment with H₂O₂ 500 μ M for 30 min, the cells were incubated with 10 μ M DHE. Subsequently, cells were resuspended with PBS, and ROS was detected by CytoFLEX S (Beckman Coulter Life Sciences, USA).

Cell death detection assays

The detection of cell death was performed with Annexin V-FITC Apoptosis Detection Kit (KGA107, KeyGEN BioTECH) and CytoFLEX S (Beckman Coulter Life Sciences, USA).

RNA isolation and quantitative real-time PCR

According to our previous study, we performed RT-qPCR assays (Hu et al, 2021). Total RNA extraction was performed by HiPure

Total RNA Plus Micro Kit (R4122-02, Magen), and reverse transcription assays were performed by HiScript[®] II Q RT SuperMix (R223-01, Vazyme) in ProFlex[™] PCR system (ThermoFisher, USA) according to manufacturer's instructions. Real-time quantitative PCR assays were performed with ChamQ Universal SYBR qPCR Master Mix (Q711-02, Vazyme) in QuantStudio[™] 5 Real-Time PCR System (ThermoFisher, USA).

The primers sequences were provided as follows:

Human

PHB1: 5'-ACCACGTAATGTGCCAGTCA-3' (Forward), 5'-TAGT CCTCTCCGATGCTGGT-3' (Reverse)

PHB2: 5'-CGGGCCCAATTCTTGGTAGA-3' (Forward), 5'-TCTGGGC TGCTCGAATCTTG-3' (Reverse)

IL1B: 5'-CCCTGCAGCTGGAGAGTGTGG-3' (Forward), 5'-TGTGCT CTGCTTGAGGTGCT-3' (Reverse)

IL6: 5'-TAGTCCTTCTACCCCAATTTCC-3' (Forward), 5'-TTGGTCC TTAGCCACTCCTTC-3' (Reverse)

GAPDH: 5'-GAGTCAACGGATTTGGTCGT-3' (Forward), 5'-GACA AGCTTCCCCTTCTCAG-3' (Reverse)

Mouse

Phb1: 5'-TCCCTTGGGTACAGAAACCAATTA-3' (Forward), 5'-TGT GATATTGACGTTCTGCA AGTCT-3' (Reverse)

Phb2: 5'-AGCAGGAACAGCACAGAAGA-3' (Forward), 5'-CGGAGCT TGATATAGCCAGGAT-3' (Reverse)

Il1b: 5'-TGACGGACCCAAAAGATGA-3' (Forward), 5'-CTGCTGC GAGATTGAAGCT-3' (Reverse)

Il6: 5'-CCCAATTTCCAATGCTCTCC-3' (Forward), 5'-CGCACTAG GT TTGCCGAGTA-3' (Reverse)

Actb: 5'-GATTACTGCTCTGGCTCCTAG-3' (Forward), 5'-GACTCAT CGTACTCCTGCTTG-3' (Reverse)

Isg15: 5'-CTAGAGCTAGAGCCTGCAG-3' (Forward), 5'-AGTTAGTCA CGGACACCAG-3' (Reverse)

Cxcl10: 5'-CCAAGTGCTGCCGTCATTTTC-3' (Forward), 5'-3'GGCT CGCAGGGATGATTTCAA (Reverse)

Cytosolic DNA immunoprecipitation and subcellular fractionation

For the detection of mtDNA binding to NLRP3 or AIM2 in J774A.1 cells, cells were seeded at 6-wells plates with a density of 10 (Swanson *et al*, 2019) cells/well. Cells were lysed by NP-40 lysis buffer and were centrifuged at 16,215 g for 20 min at 4°C. The supernatants were collected, and the concentration of total proteins was detected with BCA kits. Samples with equal protein concentration were moved into fresh 1.5 ml EP centrifuge tubes and were incubated with anti-NLRP3 antibody or anti-AIM2 antibody for 12 h at 4°C. Protein A + G Agaroses were prewashed by PBST 3 times and were added into this tube and incubated for 3 h. DNA in immunoprecipitation products was extracted with TIANamp Genomic DNA Kit (DP403, TIANGEN).

For the detection of mtDNA in the cytosol, J774A.1, HeLa cells or PBMCs were seeded at 6-wells plates with a density of 10⁶ cells/well. Cells were incubated with 1% NP-40 on ice for 15 min. The supernatants were collected and centrifuged at 16,215 g for 15 min at 4°C. The supernatants were moved into the fresh 1.5 ml EP centrifuge tubes and the DNA was extracted with TIANamp Genomic DNA Kit. The levels of mtDNA were detected by qPCR assays.

The primers sequences were provided as follows:

Human

ND1: 5'-CACCCAAGAACAGGGTTTGT-3' (Forward), 5'-TGGCCATG GGTATGTTGTAA-3' (Reverse)

D-LOOP: 5'-CTATCACCTATTAACCACTCA-3' (Forward), 5'-TTCCG CTGTAATATTGAACGTA-3' (Reverse)

COX3: 5'-AATCCAAGCCTACGTTTTCACA-3' (Forward), 5'-TGGCCA TGGGTATGTTGTAA-3' (Reverse)

18S: 5'-TAGAGGGACAAGTGGCGTTC-3' (Forward), 5'-CGCTGAG CCAGTCAGTGT-3' (Reverse)

TERT: 5'-TCACGGAGACCAGGTTTCAA-3' (Forward), 5'-TTCAA GTGC TGTCTGATTTCAA-3' (Reverse)

Mouse

D-loop: 5'-AATCTACCATCCTCCGTGAAACC-3' (Forward), 5'-TCAG TTTAGCTACCCCAAGTTAA-3' (Reverse)

Tert: 5'-CTAGCTCATGTGTCAAGACCCTCT-3' (Forward), 5'-GCCA GCACGTTTCTCTCGTT-3' (Reverse)

Seahorse cell mitochondrial stress test assay

Mitochondrial respiration capacity of J774A.1 cells or HeLa cells with or without PHB1 ablation were detected by Seahorse Cell Mito Stress Test Assay. Before the detection, cells were seeded at XFe96 Cell Culture Microplates (102601-100, Agilent) with the concentration of 12,000 cells/80 µl per well. Seahorse XFe96 Sensor Cartridge (102601-100, Agilent) was incubated at 37°C overnight without CO₂ for hydration. Cells were washed by XF Cell Mito Stress Test Assay Medium (XF Base Medium [102353-100, Agilent] with 5.5 mM glucose [G7528, Sigma], 1.0 mM pyruvate [P5280, Sigma], 2 mM L-glutamine [25030-081, Life Technologies], adjusted pH to 7.4 at 37°C, and filtered with a 0.2 µm filter [SLGP033RB, Millipore]). Before the detection, cells were incubated with XF Cell Mito Stress Test Assay Medium for 1 h at 37°C without CO₂, and assays compounds (port A: oligomycin 1 µM, port B: FCCP 0.5 µM, port C: rotenone 0.5 µM and antimycin A 0.5 µM) were added into incubated Seahorse XFe96 Sensor Cartridge according to manufacturer's instructions. According to the instructions, the assays were performed with Agilent Seahorse XFe96 system (Agilent, USA), and the data were analyzed with Seahorse Wave Desktop and Report Generator software (Agilent, USA).

Septic shock model

For survival analysis of the septic shock model, 3–4 weeks old and sex-matched mice were then intraperitoneally (i.p.) injected with LPS at a dose of 300 mg/kg body weight. After injection, mice survival was monitored every 24 h. The total duration was 7 days.

For detection of cytokines levels in mice serum, after mice were administrated with LPS for 12 h, the serum was extracted. The levels of cytokines were measured by ELISA kits.

Mice Bone marrow cells isolation and differentiation into macrophages

8–12 weeks old and sex-matched *Phb1^{F/F}* mice and *Phb1^{MyeKO}* mice were cervically dislocated after anesthetization. Hind legs were

dislodged from the acetabulum, and paws and muscles were removed. The femur and the tibia were separated, followed by cutting off both ends of the bones. After being flushed from bones by PBS, the marrow cells were filtered through the 70 μ m cell strainer and centrifuged at 250 g for 5 min at 4°C. Cells were incubated with Red blood cells lysis buffer for 10 min at 4°C, followed by resuspended with PBS. Cells were centrifuged at 250 g for 5 min at 4°C. After being resuspended with DMEM (with 15% FBS and 20% L929 cells cultural medium), cells were seeded at 10 cm cell culture dishes at a density of 10^6 /ml and cultured for 7 days to differentiate to macrophages.

For confirming the deletion of *Phb1* gene in the genome of bone marrow cells, nucleus DNA was extracted with TIANamp Genomic DNA Kit (DP403, TIANGEN), and was detected by RT-qPCR assays with the primers as follows:

PHB1: 5'-TCCCTTGGGTACAGAAACCAATTA-3' (Forward),

5'-TGTGATATTGACGTTCTGCAAGTCT-3' (Reverse)

ACTB: 5'-GATTACTGCTCTGGCTCCTAG-3' (Forward),

5'-GACTCATCGTACTCTGCTTG-3' (Reverse)

Statistics

All continuous values were shown as means \pm SEM as legends indicated. Values between groups were analyzed by a Student's *t*-test or log-rank test by GraphPad Prism 8.2.1 (GraphPad Software, Inc., USA). A two-tail $P < 0.05$ was considered statistically significant.

Data availability

This study includes no data deposited in external repositories.

Expanded View for this article is available [online](#).

Acknowledgment

We gratefully thank Dr. Isabel Hanson for editing the manuscript and Dr. Xin Pan, Institute of Basic Medical Sciences, National Center of Biomedical Analysis for kindly providing the *4mt-RCaMPh* plasmid, and Dr. Shoufa Han, Xiamen University for the DNA dye SG-ALK. We also acknowledge the core facility of the School of Basic Medical Sciences for instrument and equipment support. This project is supported by the NSFC (No. 32170758, No. 31771531), Guangdong Province Universities and Colleges Pearl River Scholar Funded Scheme (GDUPS, 2018), open research funds from the Sixth Affiliated Hospital of the Guangzhou Medical University, Qingyuan People's Hospital, Guangzhou Ling Nan Ying Cai Project 2018, and Chuang Xin Qiang Xiao project of the Guangzhou Medical University 2019KXCTD015 to Dr. DF, and the National Natural Science Foundation of China (No. 82001205, No. 82170461) to Drs. PH and TM, the Natural Science Foundation of Guangdong (2020A1515010022) and Fundamental and Applied Fundamental Research Project of Guangzhou (202102020016) to Dr. TM.

Author contributions

Du Feng: Conceptualization; resources; supervision; funding acquisition; methodology; writing—original draft; project administration; writing—review and editing. **Hao Liu**: Formal analysis; investigation; writing—original draft; project administration. **Hualin Fan**: Formal analysis; investigation; writing—original draft; project administration. **Pengcheng He**: Formal analysis;

funding acquisition; investigation; project administration; writing—review and editing. **Haixia Zhuang**: Formal analysis; investigation; writing—review and editing. **Xiao Liu**: Formal analysis; writing—review and editing. **Meiting Chen**: Formal analysis; writing—review and editing. **Wenwei Zhong**: Formal analysis; writing—review and editing. **Yi Zhang**: Formal analysis; writing—review and editing. **Cien Zhen**: Formal analysis; writing—review and editing. **Yanling Li**: Formal analysis; writing—review and editing. **Huilin Jiang**: Formal analysis; writing—review and editing. **Tian Meng**: Funding acquisition; writing—review and editing. **Yiming Xu**: Methodology; writing—review and editing. **Guojun Zhao**: Funding acquisition; investigation; writing—review and editing.

Disclosure and competing interests statement

The authors declare that they have no conflict of interest.

References

- Allam R, Lawlor KE, Yu EC, Mildenhall AL, Moujalled DM, Lewis RS, Ke F, Mason KD, White MJ, Stacey KJ *et al* (2014) Mitochondrial apoptosis is dispensable for NLRP3 inflammasome activation but non-apoptotic caspase-8 is required for inflammasome priming. *EMBO Rep* 15: 982–990
- Angus DC, van der Poll T (2013) Severe sepsis and septic shock. *N Engl J Med* 369: 840–851
- Artal-Sanz M, Tavernarakis N (2009) Prohibitin and mitochondrial biology. *Trends Endocrinol Metab* 20: 394–401
- Bernardi P, Forte M (2015) Commentary: SPG7 is an essential and conserved component of the mitochondrial permeability transition pore. *Front Physiol* 6: 320
- Bernardi P, Forte M (2016) Commentary: the m-AAA protease associated with neurodegeneration limits MCU activity in mitochondria. *Front Physiol* 7: 583
- Billingham LK, Stoolman JS, Vasan K, Rodriguez AE, Poor TA, Szibor M, Jacobs HT, Reczek CR, Rashidi A, Zhang P *et al* (2022) Mitochondrial electron transport chain is necessary for NLRP3 inflammasome activation. *Nat Immunol* 23: 692–704
- Bonora M, Bononi A, De Marchi E, Giorgi C, Lebedzinska M, Marchi S, Patergnani S, Rimessi A, Suski JM, Wojtala A *et al* (2013) Role of the c subunit of the FO ATP synthase in mitochondrial permeability transition. *Cell Cycle* 12: 674–683
- Bonora M, Giorgi C, Pinton P (2021) Molecular mechanisms and consequences of mitochondrial permeability transition. *Nat Rev Mol Cell Biol* 23: 266–285
- Bourges I, Ramus C, Mousson de Camaret B, Beugnot R, Remacle C, Cardol P, Hofhaus G, Issartel JP (2004) Structural organization of mitochondrial human complex I: role of the ND4 and ND5 mitochondria-encoded subunits and interaction with prohibitin. *Biochem J* 383: 491–499
- Buehler U, Schulenburg K, Yurugi H, Šolman M, Abankwa D, Ulges A, Tenzer S, Bopp T, Thiede B, Zipp F *et al* (2018) Targeting prohibitins at the cell surface prevents Th17-mediated autoimmunity. *EMBO J* 37: e99429
- Chen S, Xia Y, He F, Fu J, Xin Z, Deng B, He L, Zhou X, Ren W (2020) Serine supports IL-1 β production in macrophages through mTOR signaling. *Front Immunol* 11: 1866
- Crompton M, Virji S, Ward JM (1998) Cyclophilin-D binds strongly to complexes of the voltage-dependent anion channel and the adenine nucleotide translocase to form the permeability transition pore. *Eur J Biochem* 258: 729–735

- Giorgio V, von Stockum S, Antoniel M, Fabbro A, Fogolari F, Forte M, Glick GD, Petronilli V, Zoratti M, Szabó I et al (2013) Dimers of mitochondrial ATP synthase form the permeability transition pore. *Proc Natl Acad Sci USA* 110: 5887–5892
- Guo SD, Yan ST, Li W, Zhou H, Yang JP, Yao Y, Shen MJ, Zhang LW, Zhang HB, Sun LC (2020) HDAC6 promotes sepsis development by impairing PHB1-mediated mitochondrial respiratory chain function. *Aging (Albany NY)* 12: 5411–5422
- Han S, Zhou X, Shi Y, Inventors; Xiamen University, assignee (2020) SYBR Green derivative and application thereof in mitochondria DNA fluorescent imaging. US patent CN110672572B. 2020-01-10
- He J, Cooper HM, Reyes A, di Re M, Sembongi H, Litwin TR, Gao J, Neuman KC, Fearnley IM, Spinazzola A et al (2012) Mitochondrial nucleoid interacting proteins support mitochondrial protein synthesis. *Nucleic Acids Res* 40: 6109–6121
- Holley CL, Schroder K (2020) The rOX-stars of inflammation: links between the inflammasome and mitochondrial meltdown. *Clin Transl Immunology* 9: e01109
- Hornung V, Bauernfeind F, Halle A, Samstad EO, Kono H, Rock KL, Fitzgerald KA, Latz E (2008) Silica crystals and aluminum salts activate the NALP3 inflammasome through phagosomal destabilization. *Nat Immunol* 9: 847–856
- Hu Y, Chen H, Zhang L, Lin X, Li X, Zhuang H, Fan H, Meng T, He Z, Huang H et al (2021) The AMPK-MFN2 axis regulates MAM dynamics and autophagy induced by energy stresses. *Autophagy* 17: 1142–1156
- Izzo V, Bravo-San Pedro JM, Sica V, Kroemer G, Galluzzi L (2016) Mitochondrial permeability transition: new findings and persisting uncertainties. *Trends Cell Biol* 26: 655–667
- Jackson DN, Panopoulos M, Neumann WL, Turner K, Cantarel BL, Thompson-Snipes LA, Dassopoulos T, Feagins LA, Souza RF, Mills JC et al (2020) Mitochondrial dysfunction during loss of prohibitin 1 triggers Paneth cell defects and ileitis. *Gut* 69: 1928–1938
- Jian C, Xu F, Hou T, Sun T, Li J, Cheng H, Wang X (2017) Deficiency of PHB complex impairs respiratory supercomplex formation and activates mitochondrial flashes. *J Cell Sci* 130: 2620–2630
- Jin L, Batra S, Jeyaseelan S (2017) Deletion of Nlrp3 augments survival during polymicrobial sepsis by decreasing autophagy and enhancing phagocytosis. *J Immunol* 198: 1253–1262
- Kasahima K, Sumitani M, Satoh M, Endo H (2008) Human prohibitin 1 maintains the organization and stability of the mitochondrial nucleoids. *Exp Cell Res* 314: 988–996
- Keinan N, Tyomkin D, Shoshan-Barmatz V (2010) Oligomerization of the mitochondrial protein voltage-dependent anion channel is coupled to the induction of apoptosis. *Mol Cell Biol* 30: 5698–5709
- Kim J, Gupta R, Blanco LP, Yang S, Shteinfer-Kuzmine A, Wang K, Zhu J, Yoon HE, Wang X, Kerkhofs M et al (2019) VDAC oligomers form mitochondrial pores to release mtDNA fragments and promote lupus-like disease. *Science* 366: 1531–1536
- Kleckler T, Wemmer M, Haag M, Weig A, Böckler S, Langer T, Nunnari J, Westermann B (2015) Interaction of MDM33 with mitochondrial inner membrane homeostasis pathways in yeast. *Sci Rep* 5: 18344
- Ko KS, Tomasi ML, Iglesias-Ara A, French BA, French SW, Ramani K, Lozano JJ, Oh P, He L, Stiles BL et al (2010) Liver-specific deletion of prohibitin 1 results in spontaneous liver injury, fibrosis, and hepatocellular carcinoma in mice. *Hepatology* 52: 2096–2108
- Kong B, Wang Q, Fung E, Xue K, Tsang BK (2014) p53 is required for cisplatin-induced processing of the mitochondrial fusion protein L-Opa1 that is mediated by the mitochondrial metallopeptidase Oma1 in gynecologic cancers. *J Biol Chem* 289: 27134–27145
- Levytsky RM, Bohovych I, Khalimonchuk O (2017) Metalloproteases of the inner mitochondrial membrane. *Biochemistry* 56: 4737–4746
- Li S, Li H, Zhang Y-L, Xin QL, Guan ZQ, Chen X, Zhang XA, Li XK, Xiao GF, Lozach PY et al (2020) SFTSV infection induces BAK/BAX-dependent mitochondrial DNA release to trigger NLRP3 inflammasome activation. *Cell Rep* 30: 4370–4385.e7
- McArthur K, Whitehead LW, Heddleston JM, Li L, Padman BS, Oorschot V, Geoghegan ND, Chappaz S, Davidson S, San Chin H et al (2018) BAK/BAX macropores facilitate mitochondrial herniation and mtDNA efflux during apoptosis. *Science* 359: eaao6047
- Nacarelli T, Azar A, Sell C (2014) Inhibition of mTOR prevents ROS production initiated by ethidium bromide-induced mitochondrial DNA depletion. *Front Endocrinol (Lausanne)* 5: 122
- Nakahira K, Haspel JA, Rathinam VA, Lee SJ, Dolinay T, Lam HC, Englert JA, Rabinovitch M, Cernadas M, Kim HP et al (2011) Autophagy proteins regulate innate immune responses by inhibiting the release of mitochondrial DNA mediated by the NALP3 inflammasome. *Nat Immunol* 12: 222–230
- Osman C, Haag M, Potting C, Rodenfels J, Dip PV, Wieland FT, Brügger B, Westermann B, Langer T (2009) The genetic interactome of prohibitins: coordinated control of cardiolipin and phosphatidylethanolamine by conserved regulators in mitochondria. *J Cell Biol* 184: 583–596
- Pan J, Ou Z, Cai C, Li P, Gong J, Ruan XZ, He K (2018) Fatty acid activates NLRP3 inflammasomes in mouse Kupffer cells through mitochondrial DNA release. *Cell Immunol* 332: 111–120
- Perry SW, Norman JP, Barbieri J, Brown EB, Gelbard HA (2011) Mitochondrial membrane potential probes and the proton gradient: a practical usage guide. *Biotechniques* 50: 98–115
- Ren GM, Li J, Zhang XC, Wang Y, Xiao Y, Zhang XY, Liu X, Zhang W, Ma WB, Zhang J et al (2021) Pharmacological targeting of NLRP3 deubiquitination for treatment of NLRP3-associated inflammatory diseases. *Sci Immunol* 6: eabe2933
- Riley JS, Tait SW (2020) Mitochondrial DNA in inflammation and immunity. *EMBO Rep* 21: e49799
- Riley JS, Quarato G, Cloix C, Lopez J, O'Prey J, Pearson M, Chapman J, Sesaki H, Carlin LM, Passos JF et al (2018) Mitochondrial inner membrane permeabilisation enables mtDNA release during apoptosis. *EMBO J* 37: e99238
- Rongvaux A, Jackson R, Harman CC, Li T, West AP, de Zoete MR, Wu Y, Yordy B, Lakhani SA, Kuan CY et al (2014) Apoptotic caspases prevent the induction of type I interferons by mitochondrial DNA. *Cell* 159: 1563–1577
- Schroder K, Tschopp J (2010) The Inflammasomes. *Cell* 140: 821–832
- Shanmughapriya S, Rajan S, Hoffman NE, Higgins AM, Tomar D, Nemani N, Hines KJ, Smith DJ, Eguchi A, Vallem S et al (2015) SPG7 is an essential and conserved component of the mitochondrial permeability transition pore. *Mol Cell* 60: 47–62
- Shimada K, Crother TR, Karlin J, Dagvadorj J, Chiba N, Chen S, Ramanujan VK, Wolf AJ, Vergnes L, Ojcius DM et al (2012) Oxidized mitochondrial DNA activates the NLRP3 inflammasome during apoptosis. *Immunity* 36: 401–414
- Shu L, Hu C, Xu M, Yu J, He H, Lin J, Sha H, Lu B, Engelender S, Guan M et al (2021) ATAD3B is a mitophagy receptor mediating clearance of oxidative stress-induced damaged mitochondrial DNA. *EMBO J* 40: e106283
- Steglich G, Neupert W, Langer T (1999) Prohibitins regulate membrane protein degradation by the m-AAA protease in mitochondria. *Mol Cell Biol* 19: 3435–3442

- Swanson KV, Deng M, Ting JP (2019) The NLRP3 inflammasome: molecular activation and regulation to therapeutics. *Nat Rev Immunol* 19: 477–489
- Theiss AL, Vijay-Kumar M, Obertone TS, Jones DP, Hansen JM, Gewirtz AT, Merlin D, Sitaraman SV (2009) Prohibitin is a novel regulator of antioxidant response that attenuates colonic inflammation in mice. *Gastroenterology* 137: 199–208. e1-6
- Theiss AL, Laroui H, Obertone TS, Chowdhury I, Thompson WE, Merlin D, Sitaraman SV (2011) Nanoparticle-based therapeutic delivery of prohibitin to the colonic epithelial cells ameliorates acute murine colitis. *Inflamm Bowel Dis* 17: 1163–1176
- Wang LQ, Liu T, Yang S, Sun L, Zhao ZY, Li LY, She YC, Zheng YY, Ye XY, Bao Q et al (2021) Perfluoroalkyl substance pollutants activate the innate immune system through the AIM2 inflammasome. *Nat Commun* 12: 2915
- Warren EB, Aicher AE, Fessel JP, Konradi C (2017) Mitochondrial DNA depletion by ethidium bromide decreases neuronal mitochondrial creatine kinase: implications for striatal energy metabolism. *PLoS One* 12: e0190456
- West AP, Shadel GS (2017) Mitochondrial DNA in innate immune responses and inflammatory pathology. *Nat Rev Immunol* 17: 363–375
- Woodfield K, Ruck A, Brdiczka D, Halestrap AP (1998) Direct demonstration of a specific interaction between cyclophilin-D and the adenine nucleotide translocase confirms their role in the mitochondrial permeability transition. *Biochem J* 336: 287–290
- Wu J, Sun L, Chen X, Du F, Shi H, Chen C, Chen ZJ (2013) Cyclic GMP-AMP is an endogenous second messenger in innate immune signaling by cytosolic DNA. *Science* 339: 826–830
- Xian H, Watari K, Sanchez-Lopez E, Offenberger J, Onyuru J, Sampath H, Ying W, Hoffman HM, Shadel GS, Karin M (2022) Oxidized DNA fragments exit mitochondria via mPTP- and VDAC-dependent channels to activate NLRP3 inflammasome and interferon signaling. *Immunity* 55: 1370–1385. e8
- Xie M, Yu Y, Kang R, Zhu S, Yang L, Zeng L, Sun X, Yang M, Billiar TR, Wang H et al (2016) PKM2-dependent glycolysis promotes NLRP3 and AIM2 inflammasome activation. *Nat Commun* 7: 13280
- Yu C-H, Davidson S, Harapas CR, Hilton JB, Mlodzianoski MJ, Laohamonthonkul P, Louis C, Low RRJ, Moecking J, de Nardo D et al (2020) TDP-43 triggers mitochondrial DNA release via mPTP to activate cGAS/STING in ALS. *Cell* 183: 636–649. e18
- Yun B, Lee H, Ghosh M, Cravatt BF, Hsu KL, Bonventre JV, Ewing H, Gelb MH, Leslie CC (2014) Serine hydrolase inhibitors block necrotic cell death by preventing calcium overload of the mitochondria and permeability transition pore formation. *J Biol Chem* 289: 1491–1504
- Yurugi H, Tanida S, Ishida A, Akita K, Toda M, Inoue M, Nakada H (2012) Expression of prohibitins on the surface of activated T cells. *Biochem Biophys Res Commun* 420: 275–280
- Zhang F, Fan D, Mo XN (2018) Prohibitin and the extracellular matrix are upregulated in murine alveolar epithelial cells with LPS-induced acute injury. *Mol Med Rep* 17: 7769–7773
- Zhao H, Li T, Wang K, Zhao F, Chen J, Xu G, Zhao J, Li T, Chen L, Li L et al (2019) AMPK-mediated activation of MCU stimulates mitochondrial Ca²⁺ entry to promote mitotic progression. *Nat Cell Biol* 21: 476–486
- Zhong Z, Umemura A, Sanchez-Lopez E, Liang S, Shalapour S, Wong J, He F, Boassa D, Perkins G, Ali SR et al (2016) NF- κ B restricts inflammasome activation via elimination of damaged mitochondria. *Cell* 164: 896–910
- Zhong Z, Liang S, Sanchez-Lopez E, He F, Shalapour S, Lin XJ, Wong J, Ding S, Seki E, Schnabl B et al (2018) New mitochondrial DNA synthesis enables NLRP3 inflammasome activation. *Nature* 560: 198–203
- Zhou R, Yazdi AS, Menu P, Tschopp J (2011) A role for mitochondria in NLRP3 inflammasome activation. *Nature* 469: 221–225